Title: I-KCKT allows dissection-free RNA profiling of adult *Drosophila* intestinal progenitor cells

Authors: Kasun Buddika*, Jingjing Xu*, Ishara Ariyapala, and Nicholas S. Sokol

Affiliation: Department of Biology, Indiana University, Bloomington, IN 47405, USA

* Co-first authors.

Correspondence: nsokol@indiana.edu (email)
812-856-6812 (phone)

Running Title: I-KCKT RNA profiling

Abstract

The adult Drosophila intestinal epithelium is a model system for stem cell biology, but its utility is limited by current gene expression profiling methods, particularly as applied to RNA-binding proteins. Here, we describe a new profiling method that relies upon a novel intestinal progenitor Gal4 driver, termed intestinal kickout (I-KCKT)-Gal4, that is not expressed outside the gastrointestinal tract. This method uses UV cross-linked whole animal frozen powder as its starting material to specifically immunoprecipitate the RNA cargoes of transgenic epitope-tagged RNA binding proteins expressed under I-KCKT-Gal4 control. When applied to the general mRNA binder, polyA-binding protein (PABP), we show that RNA profiles obtained by this method significantly overlap with RNA-seq profiles of progenitor cells obtained via cell sorting and have very low background noise when compared to other datasets, even though we used whole animals as starting material. We further apply this approach to two specific RNA binders, LIN28 and FMRP, and identify intestinal targets for each. We expect that this approach will be broadly applicable to the field, and enable the RNA profiling of wildtype and mutant intestinal progenitor cells from intact flies subjected to a variety of environmental conditions.

Introduction

The adult *Drosophila* intestine has become a premier model for understanding the biology and behavior of resident stem cells in their native context [1]. One key approach has been gene expression profiling of intestinal cell types to characterize molecular profiles associated with cell identity, maintenance, and differentiation under both homeostatic as well as perturbed conditions (see, for example, refs [2, 3]). This approach has relied on the manual dissection of intestines. Manual dissection is not only laborious and time-consuming but also precludes certain types of analysis that require large amounts of intact, non-degraded starting material, such as immunoprecipitation (IP). Methods such as RiboTag, for example, that rely upon the sequencing of immunoprecipitates associated with RNA-binding proteins (RBPs) to analyze post-transcriptional control mechanisms, are not currently feasible in adult Drosophila intestinal stem cells but have been critical for characterizing identity and differentiation mechanisms in other stem cell lineages [4-6]. There is therefore a need for improved methods to profile this stem cell population in Drosophila [7].

Manual dissection of intestines has been required because of the lack of tools to exclusively label and manipulate individual intestinal cell types. Such tools would enable the use of the whole fly as starting material, allowing the rapid production of large amounts of starting material. Gal4 drivers have been described that label the various individual cell types in the intestinal stem cell lineage, including the intestinal stem cells (ISCs) themselves as well as their transient progenitor cell daughters, termed enteroblasts (EB), and two differentiated cell types, enterocytes (ECs) and enteroendocrine cells (EEs) [8-10]. Such Gal4 drivers can be used to express epitope-tagged transgenic proteins specifically in these various intestinal cell types that can be immunopurified. However, these Gal4 drivers are either known or likely to be active elsewhere in the adult [11].

Here, we describe a method that uses a new intestinal progenitor Gal4 driver that is not expressed outside the intestine to profile the general transcriptome as well as specific RBP cargoes expressed in this cell type. We reasoned that an intersectional

72 approach could be used to design such a Gal4 driver. Intersectional methods enable the
73 targeting of transgenic expression to the cells in which two different enhancers are both
74 active. In a recombinase-mediated intersectional method, for example, the recombinase
75 under the control of one enhancer activates a Gal4 driver under the control of a second
76 enhancer via recombinase-mediated removal of an intervening stop cassette (Fig 1A).
77 We reasoned that such a recombinase-based method involving a pan-intestinal
78 enhancer and a progenitor enhancer might limit expression to only intestinal progenitor
79 cells. We designed our transgenes with the KD recombinase (KDR), which was recently
80 shown to mediate the excision, or “kick-out”, of sequences between KDR target (KDRT)
81 sites in *Drosophila* cells [12]. We chose to use KDR so that the resulting system could
82 be used in tandem with other recombinases, like FLP, for additional manipulation of
83 intestinal cells. Because this system is designed for intestine-specific activation of a
84 “kick-out” transgene, we referred to it as Intestinal-KiCK-ouT, or I-KCKT.
85

86 ## Results

87 **I-KCKT-Gal4 labels most intestinal progenitor cells**

88 While progenitor enhancer sequence has previously been identified in the
89 *miranda* (*mira*) gene locus [13], the availability of a defined pan-intestinal enhancer was
90 less clear. Defined enhancers for some intestine-specific genes have been reported
91 (e.g. *mex1-gal4*, *npc1b-gal4*, etc. [14, 15]), but careful inspection indicated that these
92 were either not expressed throughout the intestine or in all cell types. We therefore took
93 a candidate gene approach to identify intestine-specific genes based on gene
94 expression data reported in FlyAtlas [16], and then tested DNA fragments from those
95 genes for intestinal activity. KDR transgenes containing putative enhancer sequences
96 from either *βTrypsin* (*βTry*), *θTrypsin* (*θTry*), *κTrypsin* (*κTry*), *CG10116*, or *CG18404*,
97 were tested for intestinal activity in flies also harboring two additional transgenes, a
98 *tubulin-KDRT-stop-KDRT-Gal4::p65* "kickout" transgene and a *UAS-6XGFP* responder
99 [17]. GFP expression was monitored in both the larval and adult intestine for all resulting
100 strains except for *θTry* (Fig 1B-M); in its case, only larvae were analyzed because
101 adults of the proper genotype failed to eclose. While all strains displayed some GFP
102 expression in the larval intestine, most GFP patterns were patchy and non-uniform. In
103 the adult intestine, however, two KDR lines, *βTry*-KDR and CG10116-KDR, displayed
104 expression throughout the tissue (Fig 1H, M). Careful inspection of these two indicated
105 that CG10116-KDR was expressed in most cells throughout the midgut, raising the
106 possibility that the associated enhancer fragment was pan-intestinal-specific and could
107 be used to exclusively label adult intestinal progenitor cells.

108

109 To test this possibility, we evaluated *CG10116-KDR* activity in the intestinal
110 progenitor cells of flies harboring a *mira*-containing stop cassette transgene as well as a
111 UAS-reporter that drove a nuclear-localized GFP, *UAS-stinger-GFP* [18]. For these
112 experiments, we analyzed strains containing two different *mira*-transgenes, one
113 containing an enhanced version of Gal4 with the p65 transcriptional activation domain
114 (*I-KCKT*^{p65}) and one with a non-modified version of Gal4 (*I-KCKT*) that could be used in
115 conjunction with the Gal80-dependent temporal and regional gene expression targeting
116 (TARGET) system for conditional expression [19]. To analyze CG10116-KDR-mediated

117 expression in progenitor cells, we compared GFP expression with that of a previously
118 generated and validated progenitor reporter, *mira-His2A.mCherry.HA* [7], in each of the
119 five intestinal regions (Fig 2A-J). Quantification of the percentage of mCherry+ cells that
120 were also GFP+ indicated that ~100% of progenitor cells were labeled in all regions of *I-*
121 *KCKT* strains (Fig 2P, Q). The only two exceptions to this trend were regions 1 and 3 of
122 *I-KCKT*^{p65} intestines, where only 58.7±15.5% (n=5) and 64.4±17.0% (n=5) of progenitor
123 cells were labeled, respectively. Importantly, we also found that no GFP+ cells were
124 mCherry- in *I-KCKT*^{p65} and *I-KCKT* strains indicating that no non-progenitor cells were
125 labeled in *I-KCKT* strains. To confirm this analysis, we also compared GFP expression
126 in *I-KCKT* to a second, validated progenitor reporter, *esg-LacZ* [9], and found similarly
127 that ~100% of LacZ+ cells were also GFP+ and that 0% of GFP+ cells were LacZ- (Fig
128 S1). The only exception was region 3, where ~69.9±9.0% of LacZ+ cells were GFP+,
129 indicating that the *miranda* enhancer labels a subset of progenitors in this region.
130 Collectively, this analysis indicated that almost all progenitor cells, but few if any other
131 cells, were labeled in the intestines of *I-KCKT* strains.
132
133 **I-KCKT-Gal4 is not detected in non-intestinal tissue**
134 To determine whether intestinal progenitor cells were exclusively labeled in *I-*
135 *KCKT* adults, we performed two analyses. First, we visually inspected *UAS-6XGFP-*
136 bearing adults for GFP expression. *I-KCKT* strains displayed prominent GFP
137 fluorescence in the intestine but little, if any, elsewhere (Fig 3A, B). For comparison, we
138 analyzed in parallel three other widely used drivers known to be expressed in some or
139 all intestinal progenitor cells: a *GawB* P-element insertion in the *escargot* (*esg*) locus
140 (*esg-Gal4*), a *GawB* P-element insertion in the *Delta* (*Dl*) locus (*Dl-Gal4*), and a *Notch-*
141 responsive Gal4 reporter that contains multiple, tandem binding sites for the Grainyhead
142 and Suppressor of Hairless transcription factors (*gbe-Gal4*) [9, 10]. All three were
143 detected in the intestine (Fig 3E-G); *Dl-Gal4* and *gbe-Gal4* also displayed prominent
144 non-intestinal expression while *esg-Gal4* appeared more similar to the *I-KCKT* with
145 regard to intestinal specificity. For a more rigorous analysis, we also performed
146 comparative Western Blot analysis for GFP expression on three different protein
147 extracts generated from each strain: whole animal extract (total), extract from dissected

148 gastrointestinal tracts (intestine), and extract from all remaining non-intestinal tissue
149 (carcass) (Fig 3H). For both *I-KCKT* strains, GFP was detected in intestinal but not
150 carcass extract, and the amount in the intestine was roughly similar to the amount in the
151 total extract. In contrast, GFP was detected in both the intestine and carcass of the
152 three comparison strains, *esg-Gal4*, *Dl-Gal4*, and *gbe-Gal4*. We also tested the
153 conditional expression of *I-KCKT* by generating an *I-KCKT*^{TS} strain that harbored a
154 ubiquitously expressed, temperature sensitive Gal80 transgene (*tub-Gal80*^{TS}) and then
155 performing both analyses on resulting *I-KCKT*^{TS} flies that had been incubated at the
156 non-permissive (18°) and permissive (30°) temperatures (Fig 3H-J). This analysis
157 detected no GFP expression at the non-permissive temperature, and clear expression
158 at the permissive temperature. We note that I-KCKT-driven GFP signal can also be
159 detected in the progenitor cells of the malphigian tubules (arrowheads in Fig 3J), which
160 are *esg*$^{+}$ cells that are related to midgut progenitor cells [20]. We also note that, like
161 *esg-Gal4* but to a lesser degree, *I-KCKT-Gal4* loses its progenitor-specificity in the
162 intestinal tissue of aged animals (Fig S2). Collectively, these results indicated that,
163 unlike other commonly used progenitor drivers, I-KCKT-based expression could not be
164 detected outside the intestine.
165
166 **ISC-KCKT-Gal4 specifically labels adult intestinal stem cells**
167 To further expand on the utility of the I-KCKT system, we investigated whether I-
168 KCKT expression could be limited to either the ISC or EB subsets of progenitor cells. To
169 do so, we prepared strains in which *I-KCKT*^{TS} was combined with a Gal4-silencing
170 Gal80 transgene that contained either the EB-specific *gbe* synthetic enhancer (*gbe-*
171 *Gal80*) or a fragment from the *Delta* locus reported to be active in ISCs (*Dl*^{GMR24H06}-
172 *Gal80*) [21, 22]. We referred to these strains as *ISC-KCKT*^{TS} and *EB-KCKT*^{TS},
173 respectively. Like *I-KCKT*^{TS}, both *ISC-KCKT*^{TS} and *EB-KCKT*^{TS} activity were intestine-
174 specific based on visual and/or Western blot analysis (Fig 3C, D, H). To evaluate the
175 cell type specificity of this activity, we drove GFP expression in both strains and
176 compared it to a dual reporter combination that we verified effectively distinguishes
177 ISCs and EBs (Fig S3). These dual reporters are the progenitor marker, *mira-*
178 *His2A.mCherry.HA*, and the EB-specific marker, *3Xgbe-smGFP::V5::nls*. For this

179 analysis, we scored mCherry$^+$, V5$^-$ cells as ISCs and mCherry$^+$, V5$^+$ cells as EBs. Most
180 ISCs were specifically labeled in the *ISC-KCKT^{TS}* strain: 84.1±12.3% (n=5) of ISCs were
181 labeled whereas 11.2±10.0% (n=5) of EBs were labeled across all five regions of the
182 intestine (Fig 2K-O, R, S). In contrast, EB-specific labeling in *EB-KCKT^{TS}* was less
183 effective: 57±19.8% (n=5) % of ISCs were labeled whereas only 30.7±20.1% (n=5) % of
184 EBs were labeled across all five regions of the intestine (Fig S4). Various possibilities
185 could explain this *EB-KCKT^{TS}* result, including that the GMR24H06 enhancer fragment
186 was not active in most ISCs and/or that Gal80 activity perdured in EB cells.
187 Nevertheless, this analysis indicated that *ISC-KCKT^{TS}* specifically labeled most ISCs.
188
189 **RIP-seq of PABP using I-KCKT-Gal4 identifies progenitor expressed genes**
190 We next investigated whether these I-KCKT strains could be used to streamline
191 current methods to molecularly profile progenitor cells. Current RNA-seq profiling
192 methods that rely on *esg-Gal4*, for example, require labor-intensive dissection of
193 hundreds of intestines followed by digestion of this tissue to release labeled progenitor
194 cells for fluorescent activated cell sorting (FACS) [2, 23-25]. Given the specificity of I-
195 KCKT drivers for intestinal progenitors, we reasoned that progenitor cell RNAs could
196 alternatively be profiled from intact tissue without any disruption. To test this possibility,
197 we expressed a FLAG-tagged poly-A Binding Protein (PABP) specifically in progenitors
198 with I-KCKT, prepared whole animal extract, subjected this extract to UV crosslinking to
199 covalently link protein and RNA complexes, immunoprecipitated PABP using anti-FLAG
200 beads, recovered associated RNAs, and then prepared and analyzed libraries for deep-
201 sequencing (Fig. 4A). PABP is a general mRNA-binding protein and we verified that a
202 tagged, inducible version that had previously been used to profile mRNAs in *Drosophila*
203 photoreceptor cells was expressed in progenitor cells when crossed to I-KCKT strains
204 (Fig S5) [26]. Libraries were then prepared in duplicate from RNA extracted from total
205 animal lysates of this strain ("input") as well as the PABP immunoprecipitates (PABP
206 IP). We first comparted the differential gene expression between PABP IP and input
207 using DESeq2 [27] with a false discovery rate adjusted p-value (FDR) of < 0.05 and a
208 $\log_2$ fold change greater than one, and identified 1,661 genes enriched in the PABP IP
209 samples and 3,293 enriched in input (Fig. 4B). Representative examples of these

210 respective classes are the progenitor-enriched *esg* gene and the ovary-enriched *oskar*
211 gene (*osk*) (Fig. 4C-D). To evaluate the 1,661-enriched genes, we cross-referenced this
212 set to two published datasets. First, we compared our results to transcriptome profiles
213 obtained by Doupé, who used a DamID based method to identify progenitor-enriched or
214 EC-enriched genes [28]. Twenty percent of the 1,661 were present in Doupé's
215 progenitor-enriched genes, whereas only 4% were present in the EC-enriched set (Fig.
216 4E-F). Next, we re-analyzed published RNA-seq datasets from FACS-isolated
217 progenitors, ECs, and EEs [2], then identified progenitor enriched genes compared to
218 either ECs or EEs (FDR < 0.05 and $\log_2$ fold change > 1), and found that 31%-32% of
219 these enriched genes overlapped with genes enriched in the PABP IP (Fig. 4G-H).
220 Thus, genes most highly represented in the PABP IP include a substantial number of
221 genes previously shown to be enriched in progenitor cells.
222
223 To further evaluate the accuracy of the PABP IP dataset, we reasoned that it
224 should overall bear significant similarity to the RNA-seq profile of FAC sorted progenitor
225 cells. We therefore analyzed in parallel the PABP IP dataset and four previously
226 published RNA-seq datasets from FAC-sorted progenitor cells [2, 23-25]. Read counts
227 for all five sets were normalized using the Trimmed Mean of M-values method (TMM)
228 from edgeR to allow for accurate comparisons between samples [29]. We then looked
229 for genes common to all of these datasets that had a normalized expression value > 10,
230 and found 71% (4,966 genes out of 7,000 genes) of expressed genes in the PABP IP
231 overlapped with genes identified by all the other FACS-based datasets (Fig. 4I). To
232 assess the correlation of these six datasets, Spearman correlation matrices were
233 generated and visualized as correlograms. As a negative control for this analysis, we
234 also prepared a sixth dataset of head tissue data from FlyAtlas [16]. As expected, the
235 PABP IP correlated well with all FACS based progenitor datasets while, furthermore, all
236 five of these datasets showed a similar, low correlation with the non-intestinal dataset
237 (Fig. 4J). We then used the GeneOverlap R package to perform Fisher's exact test to
238 evaluate the statistical significance of the overlap between different datasets. In addition
239 to computing the statistical significance, this package also computes both an odds ratio
240 and a Jaccard index that indicates the association and similarity between two datasets,

241 respectively. The PABP IP scored highly in both these indices when compared to each
242 of the four FAC-sorted datasets and significantly higher than either the total input or
243 head tissue datasets, further indicating the similarity between the PABP IP and FACS-
244 based datasets (Fig. 4K). We performed one additional analysis with the FACS-based
245 datasets: first, we selected progenitor-enriched genes by comparing FACS-based data
246 to two sources of whole animal datasets, total input of the PABP experiment or
247 reanalyzed whole animal dataset from FlyAtlas (FDR < 0.05 and $\log_2$ fold change > 1)
248 and then assessed the similarity of this set to the gene set enriched in the PABP IP
249 (FDR < 0.05 and $\log_2$ fold change > 1 compared to input). As expected, PABP IP
250 enriched genes showed significant low p-values and high odds ratio and Jaccard index
251 scores strengthening the positive relationship of PABP and FACS-based datasets (Fig.
252 S6A). Altogether, this bioinformatic analysis supported a conclusion that the PABP IP
253 dataset represented the gene expression profiles of progenitor cells.
254
255 Having established that the PABP IP dataset contained progenitor genes, we
256 also sought to evaluate how much non-specific background was represented in this
257 dataset. Such noise might come from the post-lysis association of transgenic PABP with
258 mRNAs from non-progenitor cells. Hypothesizing that the most abundant transcripts in
259 the whole animal lysate might be most prone to associate with PABP post-lysis, we first
260 identified the top 10% of genes in the input based on the TMM normalized expression
261 values and found 1049 genes. Only 207 of these genes were also identified in the
262 PABP IP enriched gene set, suggesting that transcripts abundantly expressed in the
263 starting lysate were not non-specifically recovered in the IP (Fig. 4L). Supporting this
264 observation, we identified 854 genes in the input that were expected not to be present in
265 the PABP IP (Fig. S6B), and confirmed that only 4 of these transcripts were present in
266 the PABP IP enriched gene list (Fig. 4M). Finally, we again used FlyAtlas data to
267 identify genes enriched in fat body, head, ovary and testis relative to midgut and then
268 compared those tissue-enriched genes to the genes either enriched in or depleted from
269 the PABP IP. We found that odds ratio and Jaccard index scores were low for PABP-
270 enriched genes, indicating minimal overlap, and significantly higher for PABP-depleted
271 genes (Fig. 4N). As a positive control for this analysis, we performed the same

comparisons with genes enriched in the Fly Atlas midgut dataset as well as genes enriched in FACS-based progenitor dataset from Buddika et al., 2020 [30]. As expected, PABP IP enriched genes show highest association with genes enriched in FACS-isolated progenitors, and significant overlap was also observed with the midgut enriched gene list (Fig. 4N). Collectively, this analysis indicated that the PABP dataset contained minimal background noise from other tissues, likely due to the effectiveness of the crosslinking step.

As an alternative to PABP, we also tested whether this same approach could be used with HA-tagged eIF4E, a translation initiation factor known to bind the mRNA cap structure [31]. Unlike PABP, overexpression of eIF4E had no effect on progenitor cell number over time (Fig S5). First, we performed differential expression analysis between eIF4E IP and the total input from the PABP experiment using DESeq2. Using a false discovery rate corrected p-value threshold of < 0.05, and a $\log_2$ fold change threshold of > 1, we found only 751 genes to be significantly enriched in the eIF4E IP, but approximately 38% of these genes were significantly enriched in the PABP IP as well (Fig. S6C, F). Similar to the PABP IP data, the eIF4E IP data showed a significant depletion of non-intestinal tissue specific transcripts, providing more proof for the specificity of the approach (Fig. S6C). The reduced number of enriched genes in the eIF4E IP may partly be due to the use of PABP total input as the control, that only a subset of transcripts are physically associated with eIF4E, or differences in IP efficiencies due to antibodies or protein isoforms. Despite these potential shortcomings, the eIF4E gene list with normalized expression values > 10 clearly overlapped well with similar lists from FACS-based datasets or PABP IP (Fig. S6D-E). These data collectively suggest that the progenitor specificity of I-KCKT drivers will simplify the labor-intensive protocols of performing any form of a biochemical or RIP-based experiments in intestinal progenitors.

300 ## Discussion

301

302 Here we describe a method to purify the RNA cargoes associated with intestinal
303 progenitor RBPs using whole animal lysate as the starting material. Because it is Gal4-
304 based, this method will have wide applicability for profiling the general PABP- or eIF4E-
305 bound transcriptome of wildtype and, when coupled with UAS-RNAi transgenes, mutant
306 progenitor cells. In addition, it opens the possibility of molecularly characterizing the
307 progenitor targets of RBPs, a growing number of which have been shown to play critical
308 roles in progenitor cells (e.g. LIN28, FMRP, SPEN, TIS11 [32-35]). Finally, this method
309 can be used in conjunction with additional current and future Gal4-based mRNA
310 profiling methods, such as TU-tagging and ribosome profiling [36, 37], as well as
311 methods that target other classes of RNAs, including microRNAs [38]. While the method
312 is currently limited to progenitor cells, its applicability could be further expanded by
313 generating kickout transgenes that drive expression in additional intestinal cell types
314 such as EEs and ECs. While we focus on RNA profiling in this study, we also expect
315 that I-KCKT in combination with mass-spectrometry to identify and characterize protein
316 complexes and protein-protein interactions.

317

318 The I-KCKT method offers a number of advantages over current progenitor cell
319 profiling methods, which usually involve the FAC sorting of progenitor cells from
320 dissected and then mechanically disrupted intestines. The use of whole animals rather
321 than dissected intestines as starting material greatly facilitates sample preparation,
322 enabling the analysis of larger numbers of samples that could be used to test additional
323 conditions and manipulations. In addition, because sample preparation is fast, this
324 approach may effectively capture labile RNA profiles. Along these lines, the elimination
325 of the FAC sorting step will also likely improve the accuracy of results, since FAC
326 sorting is known to affect gene expression profiles likely due to the time and mechanical
327 disruption associated with this step [39, 40]. In addition, this method could make
328 molecular profiling of progenitors more accessible, since cell sorting runs can be costly
329 and the equipment is not always available.

330

331 A current key limitation of the I-KCKT method is its purification of epitope-tagged
332 UAS-based transgenic protein rather than endogenous protein. This raises the concern
333 that the transgenic protein might be expressed at higher-than-endogenous levels, which
334 might cause inappropriate interactions with non-target mRNAs. Because the TARGET
335 system controlling transgene expression is temperature sensitive, this concern can be
336 addressed by testing multiple temperatures in the permissive range to identify
337 conditions supporting physiological protein expression. As an alternative approach to
338 address this concern, our current effort is focused on modifying endogenous RBP loci to
339 contain FRT-flanked epitope tags. I-KCKT-based expression of FLP should then lead to
340 the production of epitope-tagged endogenous protein in progenitor cells that would be
341 available for eCLIP-based analysis. Thus, we expect that I-KCKT-based methods will
342 allow unprecedented analysis of RNA-based mechanisms of progenitor cells.
343

Materials and Methods

Drosophila strains and husbandry:

All fly strains were cultured on standard Bloomington *Drosophila* stock center media (https://bdsc.indiana.edu/information/recipes/bloomfood.html). Flies were reared in 18ºC, 25ºC and 29ºC incubators set for a 12hr light/dark schedule and 65% humidity. The genotypes of all strains used in this study are listed in Table S1. Transgenesis to create new strains was performed by Rainbow Transgenic Flies (Camarillo, CA) using plasmid DNA described below. Additional stocks were obtained from the Bloomington Drosophila Stock Center ({20XUAS-6XGFP}attP2, P{UAS-Stinger}2, P{tubP-Gal80[ts]}20, P{UAS-dPF}D), FlyORF ({UAS-eIF4E::3xHA}ZH-86Fb (F000955)), Steven Hou (P{Su(H)GBE-Gal4, P{GawB}Dl$^{05151-G}$), the Kyoto Drosophila Stock Center (P{GawB}NP5130), and Steve Stowers ({20XUAS-DSCP 6XGFP}attP2). For GAL80^{ts}-dependent conditional expression experiments, flies were reared at 18ºC, collected over 2 days, and then shifted to 30ºC for up to 10 days before analysis. The following strains have been deposited at the Bloomington Drosophila Stock Center: (**i**) *I-KCKT^{p65}* (BDSC #. Full genotype: *mira-KDRT>-dSTOP-KDRT>-Gal4::p65^{1126}}attP40* ; *{CG10116-KD::PEST^{1107}}attP2*), (**ii**) *I-KCKT* (BDSC #. Full genotype: *{mira -KDRT>-dSTOP-KDRT>-Gal4^{1438}}attP40, P{tubP-Gal80[ts]}20 ; {CG10116-KD::PEST^{1107}}attP2*), (**iii**) *ISC-KCK^{TS}* (BDSC #. Full genotype*: {gbe-Gal80}ZH-2A ; {mira -KDRT>-dSTOP-KDRT>-Gal4^{1438}}attP40, P{tubP-Gal80[ts]}20 ; {CG10116-KD::PEST^{1107}}attP2*).

Transgenes:

KD enhancer transgenes: PCR products containing enhancer fragments amplified from genomic DNA were cloned into the HindIII and AatII sites of pJFRC161 (20XUAS-IVS-KD::PEST, a gift from Gerald Rubin, Addgene plasmid # 32140) using HiFi DNA Assembly Mix (E2621L, New England Biolabs). Oligo pairs used to amplify enhancer fragments from *βTry* (3437/3438), *θTry* (3439/3440), *κTry* (3446/3447), *CG18404* (3443/3444 for the 2.6 kb fragment, 3445/3443 for the 0.5kb fragment), and *CG10116* (3441/3442) are shown in parentheses, and oligo sequences are reported in Table S2. Junctions of resulting plasmids were verified by sequencing prior to the preparation of

375 plasmid DNA for transgenesis. KD enhancer transgenes were inserted into the attP2
376 landing site.
377
378 *KDRT Gal4 transgenes*: pJFRC164 (pJFRC164-21XUAS-KDRT>-dSTOP-KDRT>-
379 myr::RFP, a gift from Gerald Rubin, Addgene plasmid # 32141) was used as a
380 backbone for KDRT-flanked stop cassette plasmids. Four-way HiFi DNA Assembly
381 reactions were performed with (i) 7.2kb HindIII/XbaI-digested pJFRC164 plasmid
382 backbone, (ii) 1.4kb AatII/XhoI-digested pJFRC164 KDRT>-dSTOP-KDRT fragment, (iii)
383 PCR-amplified Gal4-containing fragments, and (iv) PCR amplified enhancer-containing
384 fragments. Gal4::p65 was amplified from pBPGAL4.2::p65Uw (a gift from Gerald Rubin,
385 Addgene plasmid # 26229) with oligo pair 3433/3434, while Gal4 sequence was
386 amplified from pBPGAL4.1Uw (a gift from Gerald Rubin, Addgene plasmid # 26226)
387 with oligo pair 4401/4402. Enhancer fragments include: (i) 2.6 kb *tubulin* fragment
388 amplified with oligo pair 3626/3627, (ii) 2.6 kb 5' and 1.6 kb 3' *miranda* fragments
389 amplified with oligo pairs 3489/3490 and 3491/3492, respectively, and (iii) 3.4 kb *delta*
390 fragment amplified with oligo pair 3431/3432. Plasmid junctions and open reading
391 frames were verified by sequencing prior to the preparation of DNA for transgenesis.
392 Oligo sequences are reported in Table S2, and complete plasmid sequences are
393 available upon request. KDRT transgenes were inserted into the attP40 landing site.
394
395 *Gal80 transgenes*: For DI^{R24H06}-Gal80, the previously defined R24H06 enhancer
396 fragment of the *delta* locus was PCR amplified from genomic DNA and subcloned
397 upstream of the Gal80 open reading frame in a pATTB-containing transformation
398 plasmid. 3xgbe-Gal80 was generated in a similar manner except using oligos encoding
399 three tandem copies of *gbe* sequence. Both of these Gal80 transgenes were inserted
400 into the ZH-2A landing site.
401
402 ***Dissections and immunostaining:***
403 Adult female flies were dissected in ice cold 1xPBS and fixed in 4% paraformaldehyde
404 (Electron Microscopy Sciences, Cat. No. 15714) in PBS for 45 min. Resulting dissected
405 tissue was washed in 1xPBT (1xPBS, 0.1% Triton X-100) and then blocked (1xPBT,

406 0.5% Bovine Serum Albumin) for at least 45 min. For Delta staining, an alternative
407 sample preparation scheme, adapted from [41], was followed. Briefly, intestines were
408 dissected in ice-cold Grace's Insect Medium (Lonza Bioscience, 04-457F) and fixed in a
409 1:1 (V/V) mixture of heptane (Sigma, H2198) and 4% paraformaldehyde (Electron
410 Microscopy Sciences, Cat. No. 15714) in water for 15 min. The bottom aqueous
411 paraformaldehyde layer was removed, 500µl of ice-cold methanol was added, and
412 shook vigorously for 30 seconds. The methanol/heptane mixture was removed and
413 incubated with 1ml ice-cold methanol for 5 min. Next, samples were gradually
414 rehydrated with a series of 0.3% PBT (1xPBS, 0.3% Triton X-100) : Methanol (3:7, 1:1,
415 7:3) washes, washed with 0.3% PBT alone for another 5 min and blocked (0.3% PBT,
416 0.5% Bovine Serum Albumin) for at least 45 min. Samples were incubated at 4°C
417 overnight with primary antibodies, including rabbit anti-RFP (Clontech, 1:1000), mouse
418 anti-V5 (MCA1360GA, Bio-Rad, 1:250), chicken anti-LacZ (ab9361, Abcam, 1:2000),
419 mouse anti-FLAG (F3165, Sigma, 1:1000), mouse anti-Delta (C594.9B, Developmental
420 Studies Hybridoma Bank, 1:500), and rabbit anti-HA (3724S, Cell Signaling Technology,
421 1:1000). The following day, samples were washed in 1xPBT and incubated for 2-3
422 hours with secondary antibodies, including AlexaFluor-488 and -568-conjugated goat
423 anti-rabbit, -mouse, -rat and -chicken antibodies (Life Technologies, 1:1000). Finally,
424 samples were washed in 1xPBT, including one wash with DAPI (1:1000), and mounted
425 in Vectashield mounting medium (Vector Laboratories) or, for Delta staining, in ProLong
426 Diamond mounting medium (Invitrogen, P36970).
427
428 ***Microscopy and image processing:***
429 Images of whole flies were collected on a Zeiss Axio Zoom microscope and images of
430 dissected intestines were collected on a Leica SP8 Scanning Confocal microscope.
431 Samples to be compared were collected under identical settings on the same day,
432 image files were adjusted simultaneously using Adobe Photoshop CC, and figures were
433 assembled using Adobe Illustrator CC.
434
435 ***Western blot analysis:***

436 Female *Drosophila* flies were used for protein isolation. Extract was prepared from
437 either whole animals or separately from the intestines and remaining carcass tissue of
438 dissected animals. Tissues were lysed in protein lysis buffer (25mM Tris-HCl pH 7.5,
439 150mM KCl, 5mM $MgCl_2$, 1% NP-40, 0.5mM DTT, 1xprotease inhibitor cocktail), protein
440 extracts were resolved on a 4-20% gradient polyacrylamide gel (Bio-Rad, Cat. No. 456-
441 1093), transferred to Immobilon®-P membrane (Millipore, Cat. No. IPVH00010) and
442 probed with rabbit anti-GFP (ab290, Abcam, 1:10,000) or mouse anti-a-tubulin (12G10,
443 Developmental Studies Hybridoma Bank, 1:1000) antibodies. Subsequently, blots were
444 washed extensively with 1xTBST (1xTBS, 0.1% Tween-20) and incubated with anti-
445 rabbit or -mouse conjugated HRP secondary antibodies. After extensive secondary
446 washes with 1xTBST, blots were treated with ECL-detection reagents (Thermo
447 Scientific, Cat. No. 1859701 and 1859698) and finally exposed to chemiluminescence
448 films (GE Healthcare, Cat. No. 28906839).
449
450 ***RNA immunoprecipitation and Library construction:***
451 Whole flies were collected and immediately snap frozen in liquid nitrogen and
452 stored at -80°C until sample preparation. Two hundred flies (100 male and 100 female)
453 of each sample were ground into a fine powder using a pre-cooled mortar and pestle on
454 dry ice. The powder was irradiated three times at 120 mJ per cm2 in a UV cross-linker,
455 with mixing between each irradiation cycle to maximize surface exposure. The fly
456 powder was transferred to a 2ml tube containing 1ml lysis buffer using a cold spatula,
457 and the remaining fly powder was washed off the spatula with an additional 1ml lysis
458 buffer. Tubes were incubated on ice for 15-30 min, with mixing every 5 min. Epitope-
459 tagged proteins were immunoprecipitated with either anti-Flag (Sigma) or anti-HA
460 (Pierce) magnetic beads and following the manufacturer's instructions. RNA was eluted
461 from the beads with Proteinase K and TRIzol LS Reagent was used to isolate
462 immunoprecipitated RNA. The Ovation SoLo RNA-Seq System was used to make
463 PABP and EIF4E libraries. eCLIP libraries were generated by following the protocol in
464 Nostrand et al., 2016 [42], with a minor modification that 8U of RNAse I was used per
465 sample.
466

467 ***RNA-seq data analysis***

468 RNA-seq read files were processed and aligned to the Berkeley *Drosophila*
469 Genome Project (BDGP) assembly release 6.28 (Ensembl release 99) reference
470 genome using a python based in house pipeline (https://github.com/jkkbuddika/RNA-
471 Seq-Data-Analyzer). Briefly, the quality of raw sequencing files was assessed using
472 FastQC [43] version 0.11.9, low quality reads were removed using Cutadapt [44]
473 version 2.9, reads aligning to rRNAs were removed using TagDust2 [45] version 2.2,
474 remaining reads were mapped to the Berkeley *Drosophila* Genome Project (BDGP)
475 assembly release 6.28 (Ensembl release 99) reference genome using STAR [46]
476 genome aligner version 2.7.3a and deduplicated using SAMtools [47] version 1.10.
477 Subsequently, the aligned reads were counted to the nearest overlapping feature suing
478 the Subread [48] version 2.0.0 function *featureCounts*. Finally, bigWig files representing
479 RNA-seq coverage were generated using deepTools [49] version 3.4.2 with the settings
480 --normalizeUsing CPM --binSize 1. The TMM-normalized expression values were
481 computed using the Bioconductor package edgeR [29] version 3.28.1. Differential gene
482 expression analysis was performed with the Bioconductor package DESeq2 [27] version
483 1.26.0.

484

485 ***Enhanced-CLIP (eCLIP) data analysis***

486 The eCLIP read file processing, alignment and processing was done using an
487 easy to use python based in house analysis pipeline, eCLIP data analyzer
488 (https://github.com/jkkbuddika/eCLIP-Data-Analyzer). While the eCLIP data analyzer
489 pipeline permits analysis in both paired and single-end modes, we performed all our
490 analyzes using the single-end mode, which uses only R2 read for analysis. The eCLIP
491 data analyzer pipeline performs the following steps: (1) read quality assessment using
492 FastQC [43], (2) trimming of universal eCLIP adaptors using Cutadapt [44], (3) addition
493 of UMI sequence (5'-NNNNNNNNNN in the R2 read) using UMI-tools [50] to read name
494 to facilitate PCR duplicate removal, (4) removal of reads aligning to rRNAs using
495 Tagdust2 [45], (5) alignment of remaining reads to the provided genome (i.e., BDGP
496 assembly release 6.28, Ensembl release 100) using STAR [46], (6) coordinating sort
497 and index alignment outputs using SAMtools [47], (7) removal of PCR duplicates using

498 UMI-tools [50], (8) generation of bigwig files representing RNA-seq coverage tracks
499 using deepTools [49], (9) quantification of nearest overlapping features using Subread
500 [48] function *featureCounts*, and (10) peak calling using PureCLIP [51]. All programs,
501 versions and dependencies required to execute the eCLIP data analyzer are described
502 in the user guide and can be installed using miniconda. Input normalized peak calling
503 output files were processed as described in [52]. Differential gene expression analysis
504 was performed with the Bioconductor package DESeq2 [27] version 1.26.0.
505
506 ***Statistical analysis:***
507 All statistical analyses were performed using Prism (GraphPad, Version 7.0). Datasets
508 were tested for normality using D'Agostino-Pearson test. Comparisons of two datasets,
509 were performed with an Unpaired t-test. Unless otherwise noted, significance is
510 indicated as follows: n.s., not significant; *$p < 0.05$; **$p < 0.01$; ***$p < 0.001$; ****$p <$
511 0.0001.

Acknowledgements

We thank Steven Hou, Gerald Rubin, Steve Stowers, the Kyoto Drosophila Stock Center, the Bloomington Drosophila Stock Center (supported by grant NIHP4OOD018537), the Drosophila Genome Resource Center (supported by grant NIH2P40OD010949), and the Developmental Studies Hybridoma Bank for reagents; the Light Microscopy Imaging Center (supported by grant NIH1S10OD024988-01) for access to the SP8 confocal; the Center for Genomics and Bioinformatics for sequencing results; and the National Institute of General Medical Sciences (Award R01GM124220) for financial support. The authors declare no competing financial interests.

521 **References:**

522

523 1. Li, H. and H. Jasper, *Gastrointestinal stem cells in health and disease: from flies*
524 *to humans.* Dis Model Mech, 2016. **9**(5): p. 487-99.
525 2. Dutta, D., et al., *Regional Cell-Specific Transcriptome Mapping Reveals*
526 *Regulatory Complexity in the Adult Drosophila Midgut.* Cell Rep, 2015. **12**(2): p.
527 346-58.
528 3. Hung, R.J., et al., *A cell atlas of the adult Drosophila midgut.* Proc Natl Acad Sci
529 U S A, 2020. **117**(3): p. 1514-1523.
530 4. Baser, A., et al., *Onset of differentiation is post-transcriptionally controlled in*
531 *adult neural stem cells.* Nature, 2019. **566**(7742): p. 100-104.
532 5. Sanz, E., et al., *Cell-type-specific isolation of ribosome-associated mRNA from*
533 *complex tissues.* Proc Natl Acad Sci U S A, 2009. **106**(33): p. 13939-44.
534 6. Tahmasebi, S., M. Amiri, and N. Sonenberg, *Translational Control in Stem Cells.*
535 Front Genet, 2018. **9**: p. 709.
536 7. Buddika, K., et al., *Canonical nucleators are dispensable for stress granule*
537 *assembly in Drosophila intestinal progenitors.* J Cell Sci, 2020. **133**(10).
538 8. Jiang, H. and B.A. Edgar, *EGFR signaling regulates the proliferation of*
539 *Drosophila adult midgut progenitors.* Development, 2009. **136**(3): p. 483-93.
540 9. Micchelli, C.A. and N. Perrimon, *Evidence that stem cells reside in the adult*
541 *Drosophila midgut epithelium.* Nature, 2006. **439**(7075): p. 475-9.
542 10. Zeng, X., C. Chauhan, and S.X. Hou, *Characterization of midgut stem cell- and*
543 *enteroblast-specific Gal4 lines in drosophila.* Genesis, 2010. **48**(10): p. 607-11.
544 11. Biteau, B., et al., *Lifespan extension by preserving proliferative homeostasis in*
545 *Drosophila.* PLoS Genet, 2010. **6**(10): p. e1001159.
546 12. Nern, A., et al., *Multiple new site-specific recombinases for use in manipulating*
547 *animal genomes.* Proc Natl Acad Sci U S A, 2011. **108**(34): p. 14198-203.
548 13. Bardin, A.J., et al., *Transcriptional control of stem cell maintenance in the*
549 *Drosophila intestine.* Development, 2010. **137**(5): p. 705-14.
550 14. Phillips, M.D. and G.H. Thomas, *Brush border spectrin is required for early*
551 *endosome recycling in Drosophila.* J Cell Sci, 2006. **119**(Pt 7): p. 1361-70.
552 15. Voght, S.P., et al., *Drosophila NPC1b promotes an early step in sterol absorption*
553 *from the midgut epithelium.* Cell Metab, 2007. **5**(3): p. 195-205.
554 16. Leader, D.P., et al., *FlyAtlas 2: a new version of the Drosophila melanogaster*
555 *expression atlas with RNA-Seq, miRNA-Seq and sex-specific data.* Nucleic Acids
556 Res, 2018. **46**(D1): p. D809-D815.
557 17. Shearin, H.K., et al., *Hexameric GFP and mCherry reporters for the Drosophila*
558 *GAL4, Q, and LexA transcription systems.* Genetics, 2014. **196**(4): p. 951-60.
559 18. Barolo, S., L.A. Carver, and J.W. Posakony, *GFP and beta-galactosidase*
560 *transformation vectors for promoter/enhancer analysis in Drosophila.*
561 Biotechniques, 2000. **29**(4): p. 726, 728, 730, 732.
562 19. McGuire, S.E., Z. Mao, and R.L. Davis, *Spatiotemporal gene expression*
563 *targeting with the TARGET and gene-switch systems in Drosophila.* Sci STKE,
564 2004. **2004**(220): p. pl6.

565 20. Singh, S.R., W. Liu, and S.X. Hou, *The adult Drosophila malpighian tubules are*
566 *maintained by multipotent stem cells.* Cell Stem Cell, 2007. **1**(2): p. 191-203.
567 21. Guo, Z., I. Driver, and B. Ohlstein, *Injury-induced BMP signaling negatively*
568 *regulates Drosophila midgut homeostasis.* J Cell Biol, 2013. **201**(6): p. 945-61.
569 22. Furriols, M. and S. Bray, *A model Notch response element detects Suppressor of*
570 *Hairless-dependent molecular switch.* Curr Biol, 2001. **11**(1): p. 60-4.
571 23. Fast, D., et al., *Vibrio cholerae-Symbiont Interactions Inhibit Intestinal Repair in*
572 *Drosophila.* Cell Rep, 2020. **30**(4): p. 1088-1100 e5.
573 24. Korzelius, J., et al., *The WT1-like transcription factor Klumpfuss maintains*
574 *lineage commitment of enterocyte progenitors in the Drosophila intestine.* Nat
575 Commun, 2019. **10**(1): p. 4123.
576 25. Li, Q., et al., *Ingestion of Food Particles Regulates the Mechanosensing*
577 *Misshapen-Yorkie Pathway in Drosophila Intestinal Growth.* Dev Cell, 2018.
578 **45**(4): p. 433-449 e6.
579 26. Yang, Z., H.J. Edenberg, and R.L. Davis, *Isolation of mRNA from specific tissues*
580 *of Drosophila by mRNA tagging.* Nucleic Acids Res, 2005. **33**(17): p. e148.
581 27. Love, M.I., W. Huber, and S. Anders, *Moderated estimation of fold change and*
582 *dispersion for RNA-seq data with DESeq2.* Genome Biol, 2014. **15**(12): p. 550.
583 28. Doupe, D.P., et al., *Drosophila intestinal stem and progenitor cells are major*
584 *sources and regulators of homeostatic niche signals.* Proc Natl Acad Sci U S A,
585 2018. **115**(48): p. 12218-12223.
586 29. Robinson, M.D., D.J. McCarthy, and G.K. Smyth, *edgeR: a Bioconductor*
587 *package for differential expression analysis of digital gene expression data.*
588 Bioinformatics, 2010. **26**(1): p. 139-40.
589 30. Buddika, K., et al., *Intestinal progenitor P-bodies maintain stem cell identity by*
590 *suppressing pro-differentiation factors.* BioRxiV, 2020.
591 31. Rissland, O.S., *The organization and regulation of mRNA-protein complexes.*
592 Wiley Interdiscip Rev RNA, 2017. **8**(1).
593 32. Andriatsilavo, M., et al., *Spen limits intestinal stem cell self-renewal.* PLoS Genet,
594 2018. **14**(11): p. e1007773.
595 33. Chen, C.H., A. Luhur, and N. Sokol, *Lin-28 promotes symmetric stem cell*
596 *division and drives adaptive growth in the adult Drosophila intestine.*
597 Development, 2015. **142**(20): p. 3478-87.
598 34. Luhur, A., et al., *Opposing Post-transcriptional Control of InR by FMRP and LIN-*
599 *28 Adjusts Stem Cell-Based Tissue Growth.* Cell Rep, 2017. **21**(10): p. 2671-
600 2677.
601 35. McClelland, L., H. Jasper, and B. Biteau, *Tis11 mediated mRNA decay promotes*
602 *the reacquisition of Drosophila intestinal stem cell quiescence.* Dev Biol, 2017.
603 **426**(1): p. 8-16.
604 36. Chen, X. and D. Dickman, *Development of a tissue-specific ribosome profiling*
605 *approach in Drosophila enables genome-wide evaluation of translational*
606 *adaptations.* PLoS Genet, 2017. **13**(12): p. e1007117.
607 37. Hida, N., et al., *EC-tagging allows cell type-specific RNA analysis.* Nucleic Acids
608 Res, 2017. **45**(15): p. e138.

38. Luhur, A., G. Chawla, and N.S. Sokol, *MicroRNAs as components of systemic signaling pathways in Drosophila melanogaster.* Curr Top Dev Biol, 2013. **105**: p. 97-123.
39. Andra, I., et al., *An Evaluation of T-Cell Functionality After Flow Cytometry Sorting Revealed p38 MAPK Activation.* Cytometry A, 2020. **97**(2): p. 171-183.
40. Richardson, G.M., J. Lannigan, and I.G. Macara, *Does FACS perturb gene expression?* Cytometry A, 2015. **87**(2): p. 166-75.
41. Lin, G., N. Xu, and R. Xi, *Paracrine Wingless signalling controls self-renewal of Drosophila intestinal stem cells.* Nature, 2008. **455**(7216): p. 1119-23.
42. Van Nostrand, E.L., et al., *Robust transcriptome-wide discovery of RNA-binding protein binding sites with enhanced CLIP (eCLIP).* Nat Methods, 2016. **13**(6): p. 508-14.
43. Andrews, S., *FastQC: A quality control tool for high throughput sequence data.* http://wwwbioinformaticsbabrahamacuk/projects/fastqc, 2010.
44. Martin, M., *Cutadapt removes adapter sequences from high-throughput sequencing reads.* 2011, 2011. **17**(1): p. 3.
45. Lassmann, T., *TagDust2: a generic method to extract reads from sequencing data.* BMC Bioinformatics, 2015. **16**: p. 24.
46. Dobin, A., et al., *STAR: ultrafast universal RNA-seq aligner.* Bioinformatics, 2013. **29**(1): p. 15-21.
47. Li, H., et al., *The Sequence Alignment/Map format and SAMtools.* Bioinformatics, 2009. **25**(16): p. 2078-9.
48. Liao, Y., G.K. Smyth, and W. Shi, *The R package Rsubread is easier, faster, cheaper and better for alignment and quantification of RNA sequencing reads.* Nucleic Acids Res, 2019. **47**(8): p. e47.
49. Ramirez, F., et al., *deepTools2: a next generation web server for deep-sequencing data analysis.* Nucleic Acids Res, 2016. **44**(W1): p. W160-5.
50. Smith, T., A. Heger, and I. Sudbery, *UMI-tools: modeling sequencing errors in Unique Molecular Identifiers to improve quantification accuracy.* Genome Res, 2017. **27**(3): p. 491-499.
51. Krakau, S., H. Richard, and A. Marsico, *PureCLIP: capturing target-specific protein-RNA interaction footprints from single-nucleotide CLIP-seq data.* Genome Biol, 2017. **18**(1): p. 240.
52. Busch, A., et al., *iCLIP data analysis: A complete pipeline from sequencing reads to RBP binding sites.* Methods, 2020. **178**: p. 49-62.

646 **Figure Legends:**

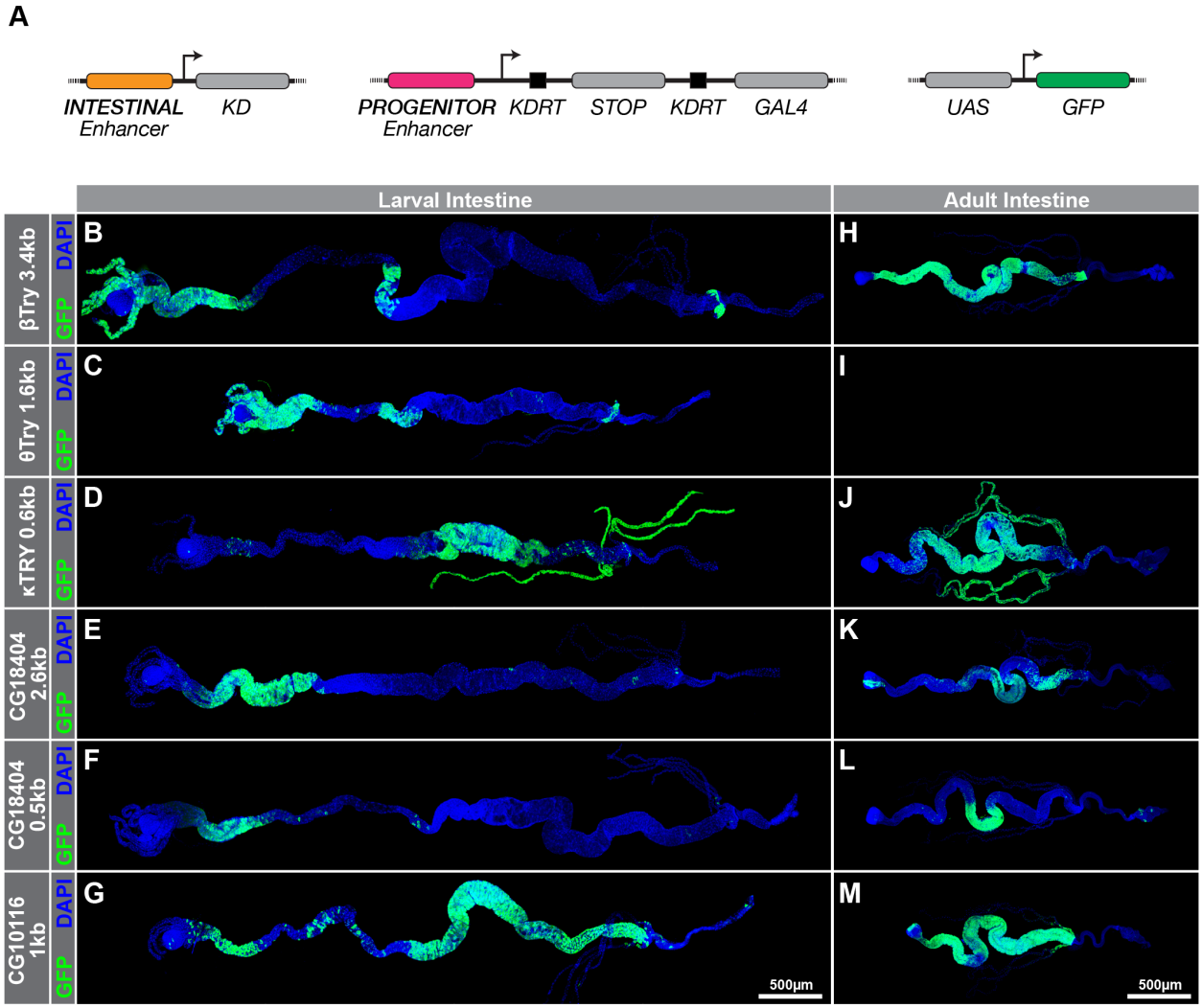

647

648 **Figure 1: KD driver analysis identifies a pan-intestinal enhancer in adults**. (A)
649 Schematic of the I-KCKT system, which involves three transgenes: (i) a KD-expressing
650 transgene under the control of an intestinal enhancer, (ii) a transgene in which a KDRT-
651 flanked stop-cassette separates Gal4 from a progenitor enhancer, and (iii) a UAS
652 responder, in this case, controlling GFP expression. (B-M) KD recombinase-mediated
653 labeling of (B-G) larval and (H-M) adult intestinal cells. KD lines contain 3.4kb *βTry*
654 (B,H), 1.6kb *θTry* (C, I), 0.6kb *κTry* (D, J), 2.6kb *CG18404* (E, K), 0.5kb *CG18404* (F, L),
655 or 1kb *CG10116* (G, M) enhancer sequences. KD expression pattern was detected
656 based on KDRT-mediated activation of a *tubulin*-based Gal4::p65 driver in combination
657 with a *UAS-6XGFP* responder. Full genotypes are listed in Table S1.

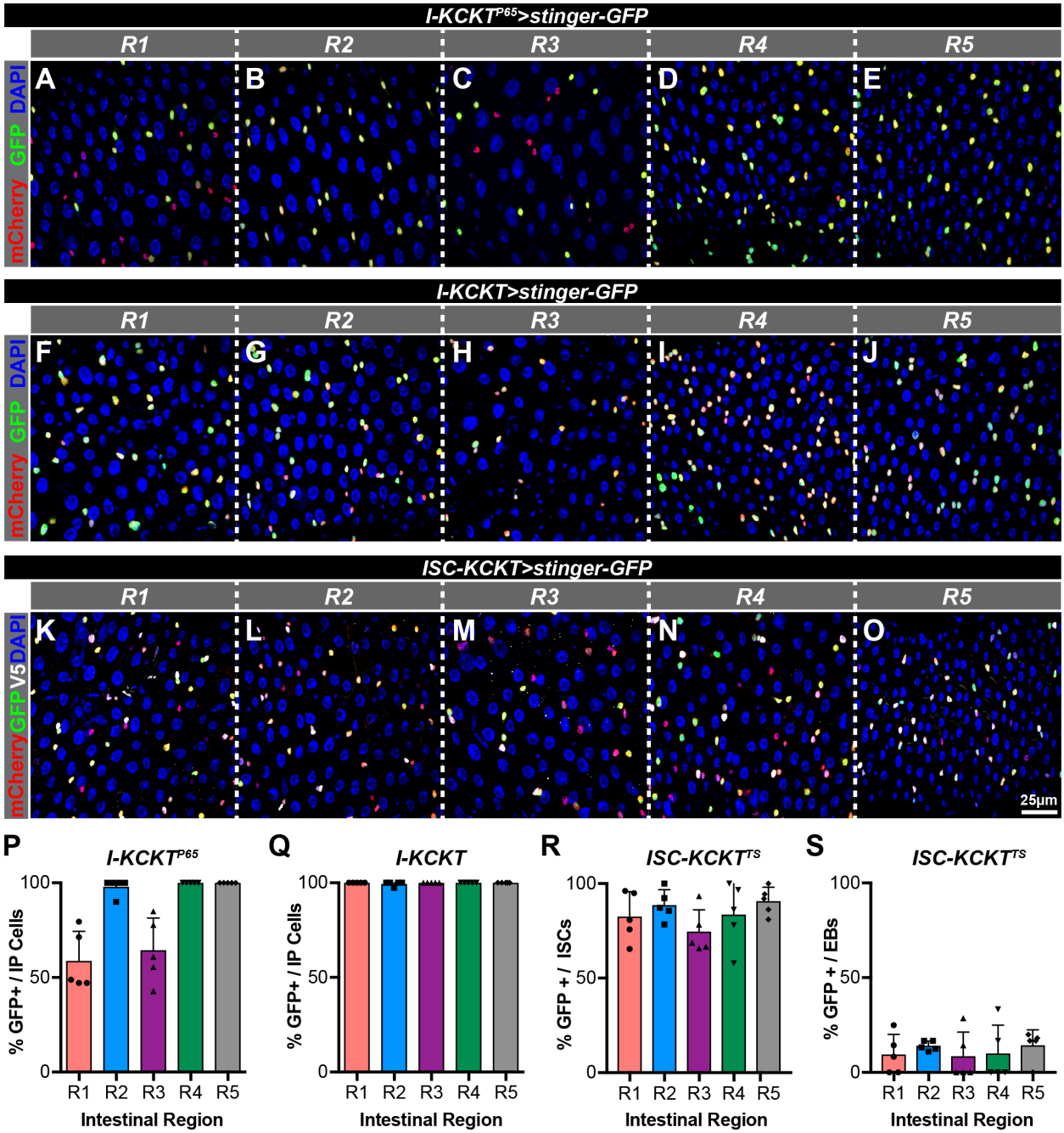

Figure 2: I-KCKT^{P65} and I-KCKT labels most intestinal progenitor cells and ISC-KCKT^{TS} labels most ISCs. (A-O) Representative micrographs of the five regions (R1-R5) from intestines stained for I-KCKT^{P65}>UAS-stinger-GFP (A-E), I-KCKT>UAS-stinger-GFP (F-J), or ISC-KCKT>UAS-stinger-GFP (K-O) in green and counterstained for intestinal progenitor marker *mira-His2A.mCherry.HA* in red and the DAPI DNA marker in blue. (P-Q) Histograms showing percentage of *mira-His2A.mCherry.HA*-

666 labeled intestinal progenitor (IP) cells that are also labeled with I-KCKT^{P65}>UAS-stinger-
667 GFP (F) or I-KCKT>UAS-stinger-GFP (L) per intestinal region (R1-R5). (R-S)
668 Histograms showing the percentage of ISCs (R) and EBs (S) labeled with ISC-KCKT^{TS}.
669 Full genotypes are listed in Table S1.
670

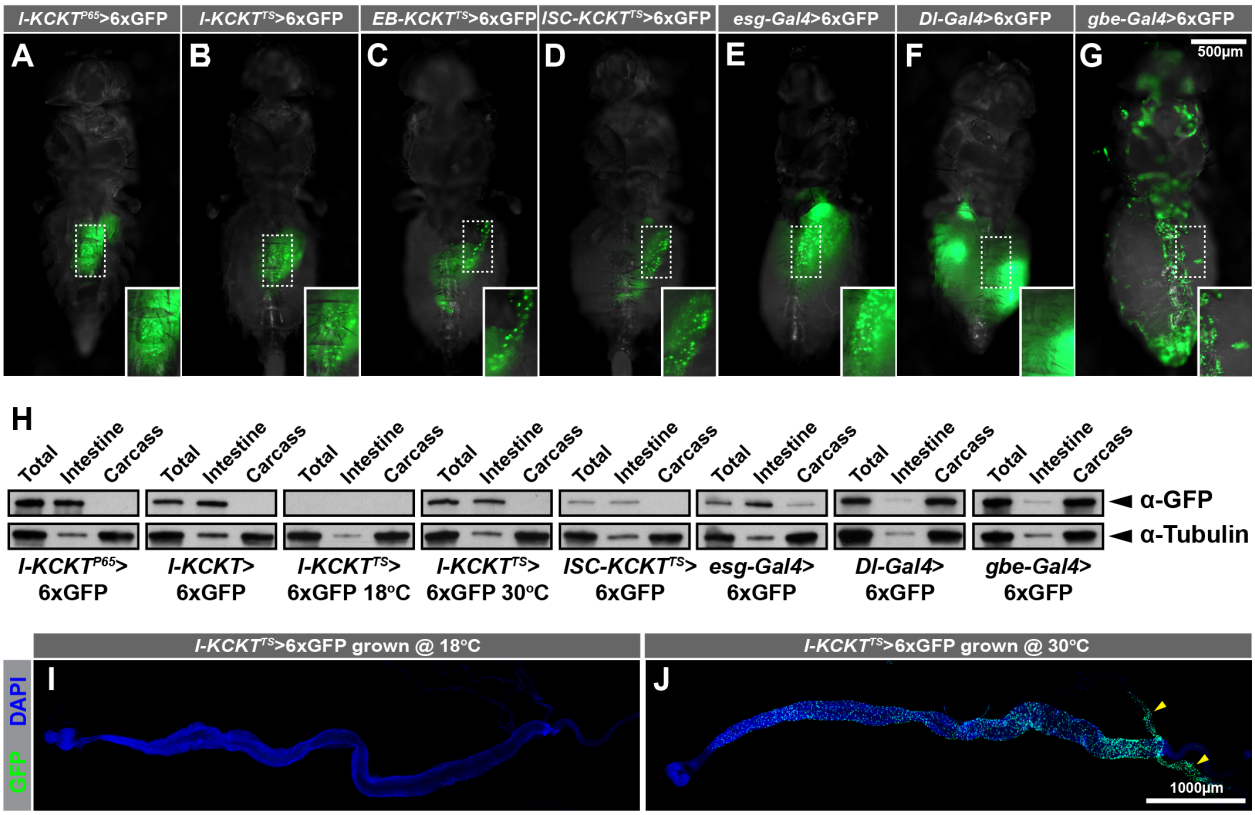

Figure 3: I-KCKT drivers are intestine-specific. (A-G) Pictures of whole adult females showing 6XGFP expression patterns driven by I-KCKT^{P65} (A), I-KCKT^{TS} (B), EB-KCKT^{TS} (C), ISC-KCKT^{TS} (D), esg$^{P\{GawB\}NP5130}$-Gal4 (E), Dl$^{05151\text{-}G}$-Gal4 (F), or Su(H)GBE-Gal4 (G) Insets are enlargements of abdominal regions displaying intestinal GFP expression. (H) Western blot analysis of tissue extracts from whole animals (total), dissected intestines, or dissected carcasses showing 6XGFP levels driven by I-KCKT^{P65}, I-KCKT, I-KCKT^{TS} at 18°C, I-KCKT^{TS} at 30°C, ISC-KCKT^{TS}, esg$^{P\{GawB\}NP5130}$-Gal4, Dl$^{05151\text{-}G}$-Gal4, or Su(H)GBE-Gal4. (I, J) 6XGFP expression in dissected intestines of I-KCKT^{TS}>6GFP adults kept at 18°C (I) or 30°C (J) and counterstained for the DAPI DNA marker in blue. Yellow arrowheads indicate GFP expression at the base of the malphigian tubules. Full genotypes are listed in Table S1.

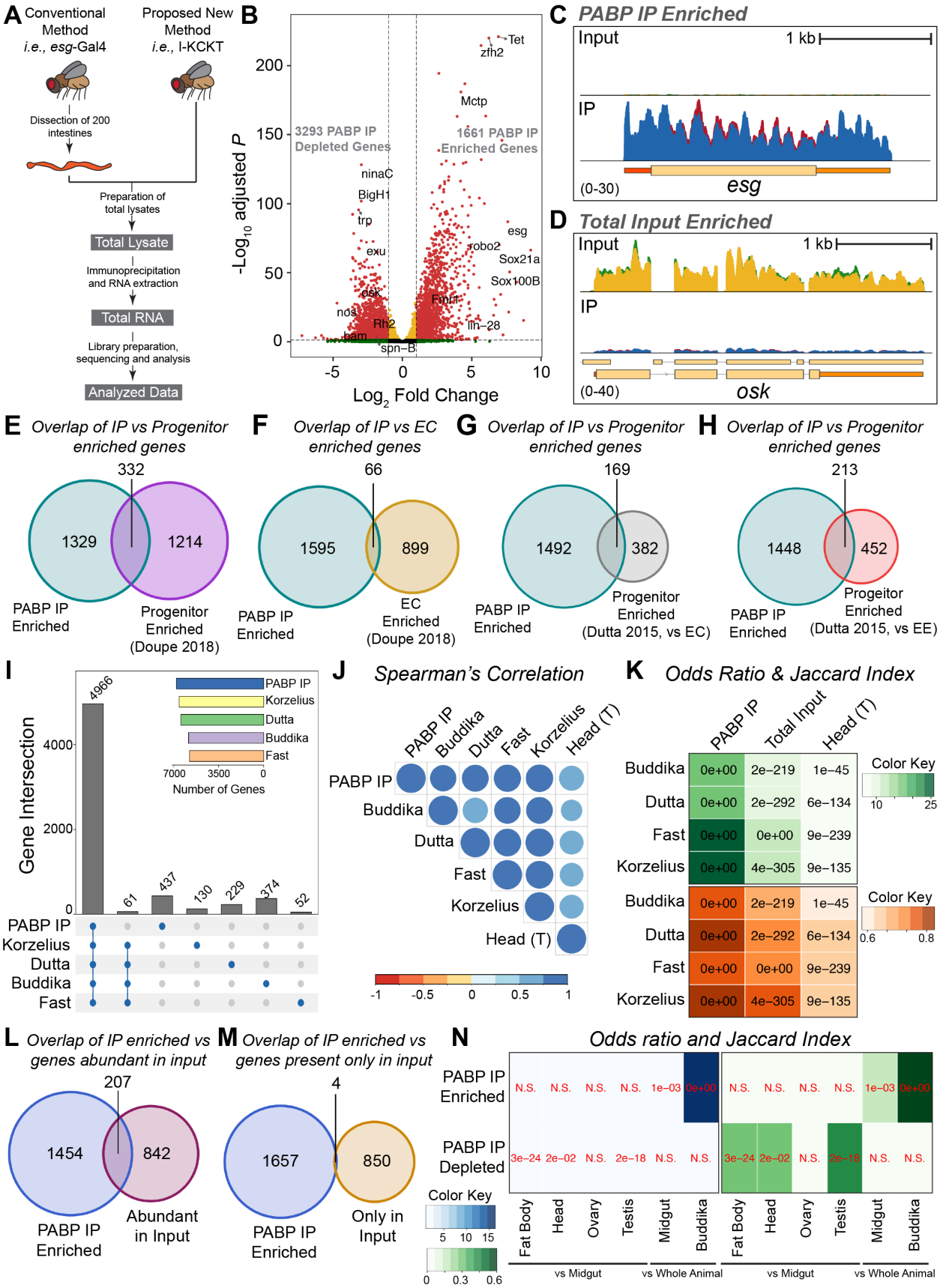
A
Conventional Method i.e., esg-Gal4
Proposed New Method i.e., I-KCKT
Dissection of 200 intestines
Preparation of total lysates
Total Lysate
Immunoprecipitation and RNA extraction
Total RNA
Library preparation, sequencing and analysis
Analyzed Data
B
3293 PABP IP Depleted Genes
1661 PABP IP Enriched Genes
Tet
zfh2
Mctp
ninaC
BigH1
trp
exu
esg
robo2
Sox21a
Sox100B
osk
Fmr1
nos
Rh2
lin-28
bam
spn-B
-Log10 adjusted P
Log2 Fold Change
C PABP IP Enriched
Input
IP
1 kb
(0-30)
esg
D Total Input Enriched
Input
IP
1 kb
(0-40)
osk
E Overlap of IP vs Progenitor enriched genes
332
1329
1214
PABP IP Enriched
Progenitor Enriched (Doupe 2018)
F Overlap of IP vs EC enriched genes
66
1595
899
PABP IP Enriched
EC Enriched (Doupe 2018)
G Overlap of IP vs Progenitor enriched genes
169
1492
382
PABP IP Enriched
Progenitor Enriched (Dutta 2015, vs EC)
H Overlap of IP vs Progenitor enriched genes
213
1448
452
PABP IP Enriched
Progeitor Enriched (Dutta 2015, vs EE)
I
Gene Intersection
Number of Genes
PABP IP
Korzelius
Dutta
Buddika
Fast
4966
61
437
130
229
374
52
J Spearman's Correlation
PABP IP
Buddika
Dutta
Fast
Korzelius
Head (T)
K Odds Ratio & Jaccard Index
PABP IP
Total Input
Head (T)
Color Key
L Overlap of IP enriched vs genes abundant in input
207
1454
842
PABP IP Enriched
Abundant in Input
M Overlap of IP enriched vs genes present only in input
4
1657
850
PABP IP Enriched
Only in Input
N Odds ratio and Jaccard Index
PABP IP Enriched
PABP IP Depleted
Fat Body
Head
Ovary
Testis
Midgut
Buddika
vs Midgut
vs Whole Animal
Color Key

686 **Figure 4: RIP-seq of PABP using I-KCKT identifies progenitor expressed genes.**
687 (A) Schematic representation of the conventional FACS (left) and I-KCKT-based
688 intestinal progenitor RNA-sequencing (right). (B) Volcano plot of differentially expressed
689 genes from comparison of PABP IP to total input. Each dot represents a single gene.
690 Yellow indicates a false discovery rate adjusted p-value (FDR) < 0.05 and a Log_2 fold
691 change > 1 or < -1. Green indicates Log_2 fold change > 1 or < -1 and an FDR >= 0.05.
692 Red indicates an FDR < 0.05 and log_2 fold change > 1 or < -1. A selected set of
693 significantly changed genes have been labeled. (C-D) Genome browser tracks of
694 normalized total input and PABP IP at the (C) *esg* or (D) *osk* locus of the *Drosophila*
695 genome. Note that the two replicates of the total input (green and yellow) and the two
696 replicates of the PABP IP (red and blue) have been overlayed for simplicity. (E-H) Venn
697 diagram of genes significantly enriched in PABP-RIP compared to total input (FDR <
698 0.05 and log_2 fold change > 1) and (E) in intestinal progenitors based on progenitor
699 DamID, or (F) in ECs based on EC DamID based on [28], or (G) in intestinal progenitors
700 compared to ECs (FDR < 0.05 and log_2 fold change > 1) or (H) in intestinal progenitors
701 compared to EEs (FDR < 0.05 and log_2 fold change > 1) based on reanalyzed data from
702 [2]. (I) Upset plot showing the overlap of moderately expressed genes identified by
703 PABP RIP-seq versus previously published FACS based methods. Only a selected set
704 of meaningful overlaps are shown for simplicity. Numbers above each bar shows the
705 size of each intersection. (J) Correlogram of Spearman's *rho* values for pairwise
706 comparisons of progenitor expressed genes based on PABP RIP-seq and FACS-based
707 progenitor RNA-seq as well as *Drosophila* female head expressed genes based on
708 RNA-seq of dissected heads. (K) Heatmaps of odds ratio (in green) and Jaccard index
709 (in orange) values for pairwise comparisons of PABP RIP-seq, RNA-seq of total input or
710 RNA-seq of dissected female heads against FACS-based progenitor RNA-seq.
711 Numbers on each colored box show the p-value for each overlap based on Fisher's
712 exact test. For I-K, PABP IP indicates data from I-KCKT-based PABP RIP-seq. Buddika,
713 Dutta, Fast and Korzelius indicate data from RNA-seq of FACS isolated progenitors
714 from [2, 23, 24, 30], respectively. For J-K, Head indicates reanalyzed female head RNA-
715 seq data from Leader *et al.,* 2017. (L-M) Venn diagram of genes significantly enriched in
716 PABP-RIP compared to total input (FDR < 0.05 and log_2 fold change > 1) and (L) top

717 10% genes with highest TMM normalized expression values or (M) genes uniquely
718 present in input, but not in any of the FACS-based RNA-seq gene lists. (N) Heatmaps of
719 odds ratio (in blue) and Jaccard index (in green) values for pairwise comparisons of
720 PABP IP enriched (FDR < 0.05 and $\log_2$ fold change > 1 vs input) or PABP IP depleted
721 (FDR < 0.05 and $\log_2$ fold change < -1 vs input) genes against fat body, head, ovary or
722 testis enriched genes compared to midgut (FDR < 0.05 and $\log_2$ fold change > 1) or
723 genes enriched in midgut or FACS-based progenitor dataset from Buddika *et al.,* 2020
724 [30] compared to whole animal input (FDR < 0.05 and $\log_2$ fold change > 1). Numbers
725 on each colored box show the p-value for each overlap based on Fisher's exact test.
726 Note that fat body, head, ovary, testis, midgut and whole animal datasets represent
727 reanalyzed data from [16].
728

729 **Supplementary Figure Legends:**

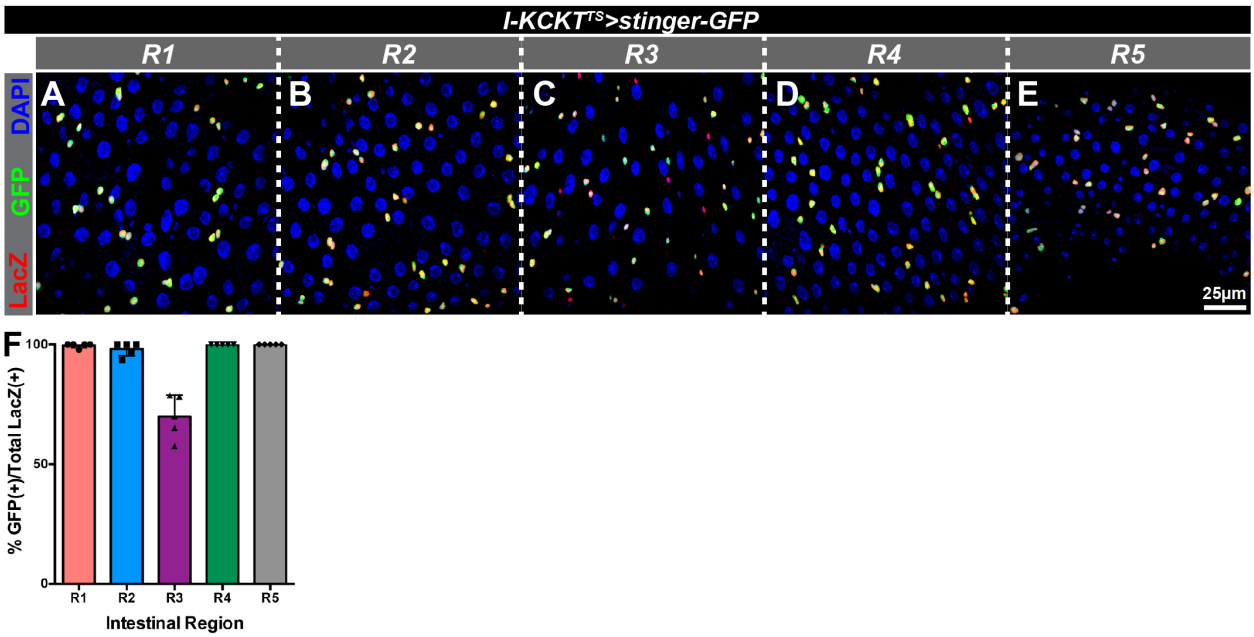

730

731

732 **Figure S1: I-KCKT and esg-LacZ label the same cells**. (A-E) Representative
733 micrographs of the five regions (R1-R5) from the intestines of 5-day old females stained
734 for *I-KCKT^{TS}>UAS-stinger-GFP* in green, *esg-LacZ* in red, and the DAPI DNA marker in
735 blue. (F) Histogram of the percentage of *esg-LacZ*-positive cells that also expressed *I-*
736 *KCKT^{TS}>UAS-stinger-GFP* in each region.

737

738

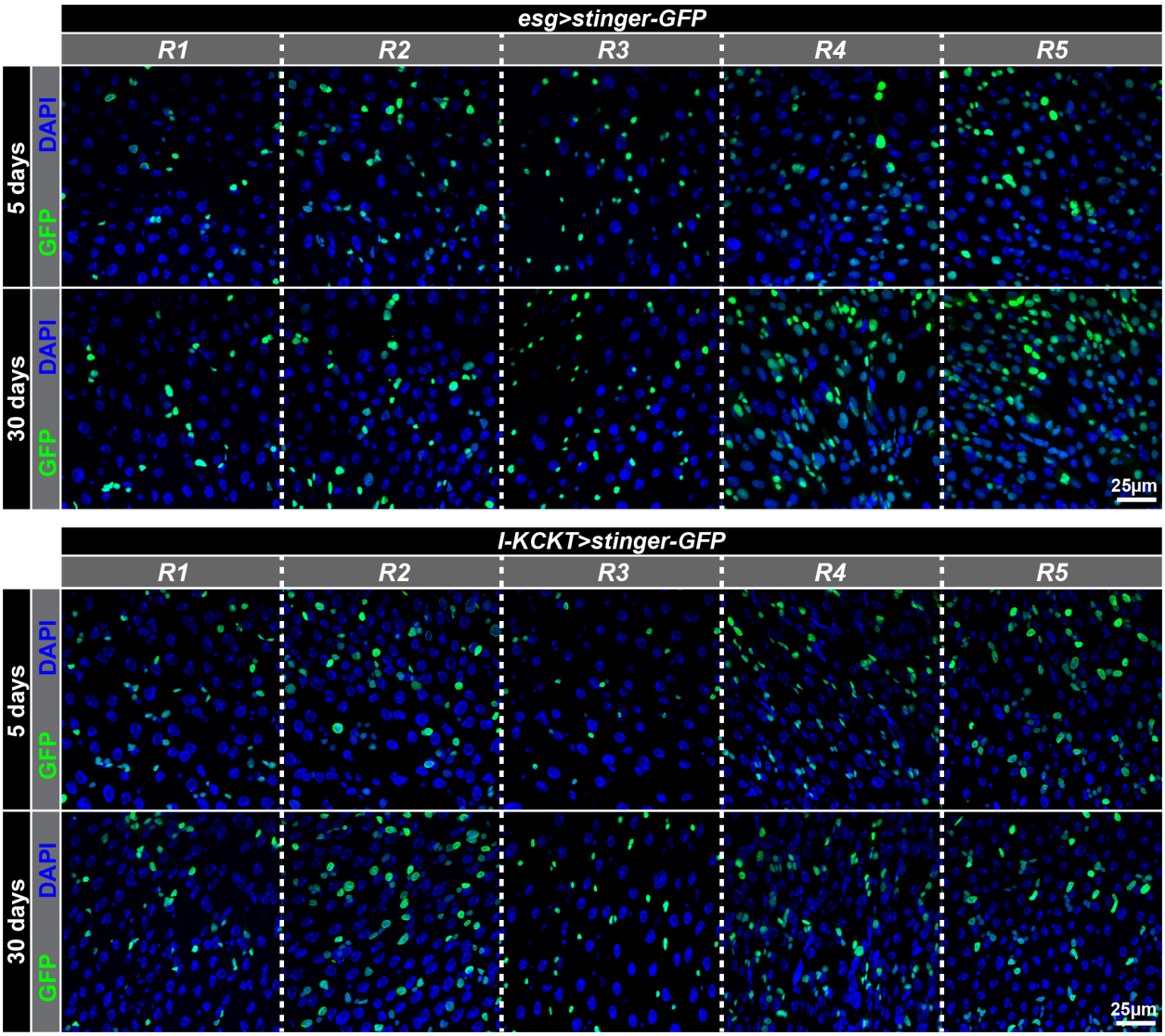

Figure S2: Comparison of I-KCKT-Gal4 and esg expression in aged flies. Representative micrographs of the five regions (R1-R5) from the intestines from young (5 day) and older (30-day) females stained for *esg>UAS-stinger-GFP* (top) or *I-KCKT^{P65}>UAS-stinger-GFP* (bottom) in green and counterstained for the DAPI DNA marker in blue.

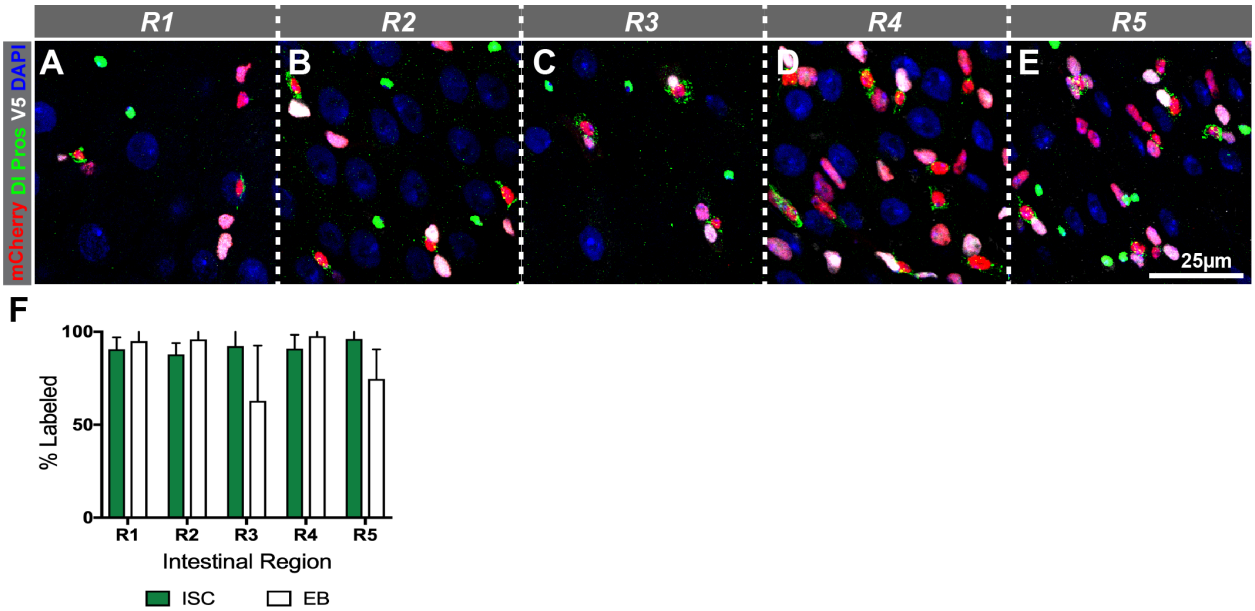

Figure S3: Verification that dual reporters *mira-His2A.mCherry.HA* and *3Xgbe-smGFP::V5::nls* effectively distinguish ISCs and EBs. (A-E) Representative micrographs of the five regions (R1-R5) from the intestines of 5-day old females stained for ISCs (anti-Delta, green cytoplasmic staining), EEs (anti-Prospero, green nuclear staining), *mira-His2A.mCherry.HA* (red), *3Xgbe-smGFP::V5::nls (white),* and the DAPI DNA marker (blue). (F) Quantification of the percent of ISCs and EBs labeled by the dual reporters *mira-His2A.mCherry.HA* and *3Xgbe-smGFP::V5::nls* in each of the five intestinal regions. ISCs were defined as the number of Delta+ cells per field of view. EBs were defined as the number of Delta-, mCherry+ cells per field of view. For quantification, field of view images were taken and quantified from defined portions of each intestinal region in 6-7 intestines. We note that we detected a few (1-5) cells that were both Delta+ and *3Xgbe-smGFP::V5::nls*+ in regions of most intestines. These were not scored as either ISCs or EBs, and could represent cells transitioning between these two cell fates.

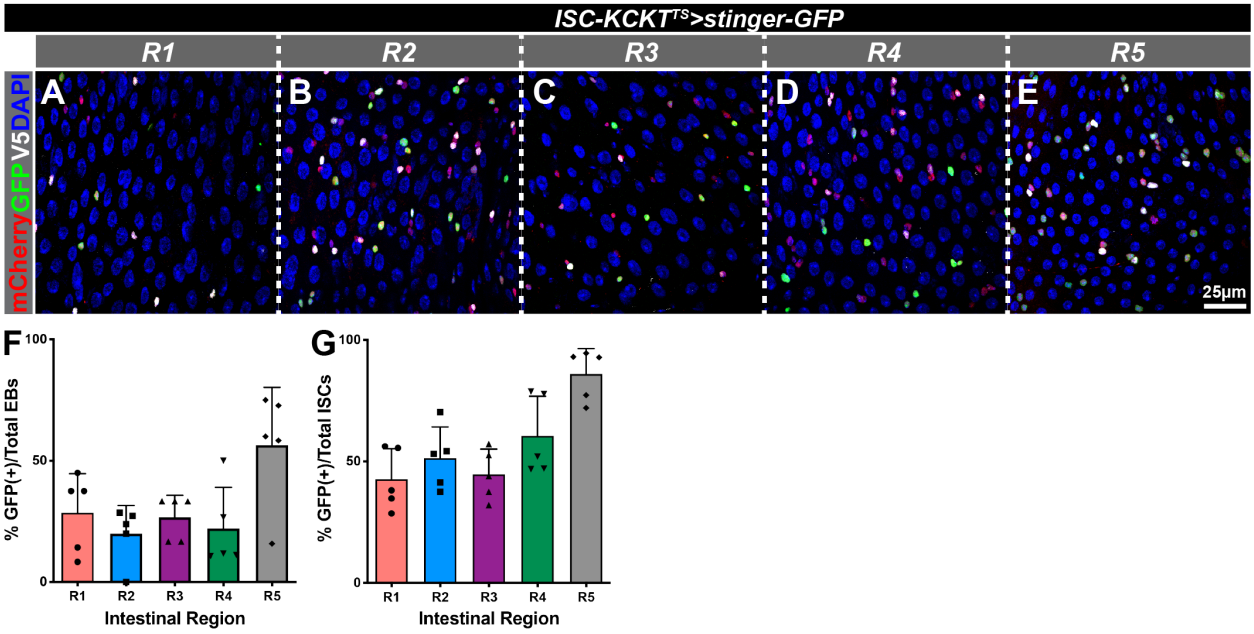

764

765

766 **Figure S4: ISC-KCKT^{TS} labels many ISCs.** (A-E) Representative micrographs of the
767 five regions (R1-R5) from the intestines of 5-day old females stained for *I-*
768 *KCKT^{TS}>UAS-stinger-GFP* in green, *mira-His2A.mCherry.HA* in red, *3Xgbe-*
769 *smGFP::V5::nls* in white, and the DAPI DNA marker in blue. ISCs were scored as cells
770 positive for *mira-His2A.mCherry.HA* and negative for *3Xgbe-smGFP::V5::nls*, while EBs
771 were scored as cells positive for both markers. (F) Histogram of the percentage of EBs that
772 expressed *I-KCKT^{TS}>UAS-stinger-GFP* in each region. (G) Histogram of the percentage
773 of ISCs that expressed *I-KCKT^{TS}>UAS-stinger-GFP* in each region.

774

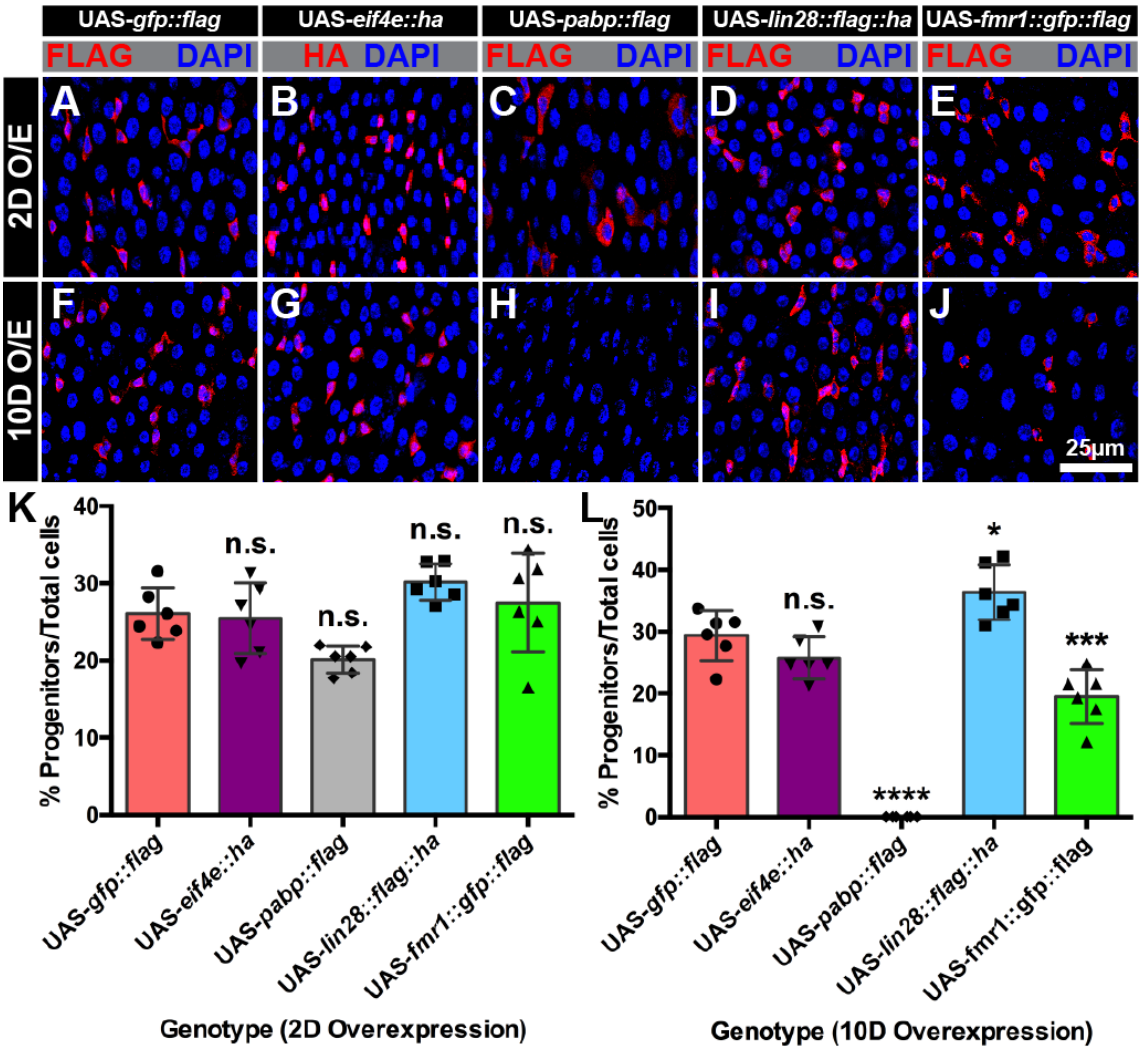

Figure S5: I-KCKT^{TS}-dependent expression of tagged RBPs in intestinal progenitor cells. (A-J) Micrographs of intestines showing I-KCKT^{TS}-dependent expression of UAS-GFP::FLAG (A, F), UAS-EIF4E::HA (D, I), UAS-PABP::FLAG (E, J), UAS-LIN28::FLAG::HA (B, G), and UAS-FMR1::GFP::FLAG (C, H) after two (A-E) and ten (F-J) days at the permissive temperature. Expressed proteins were detected with either anti-FLAG or -HA antibodies (shown in red) and intestines were counterstained with the DAPI DNA marker in blue. Full genotypes are listed in Table S1. (K, L) Histograms of the percentage of progenitor cells after two and ten days of I-KCKT^{TS}-dependent expression, based on quantification of the numbers of HA/FLAG^{+} and DAPI^{+} cells.

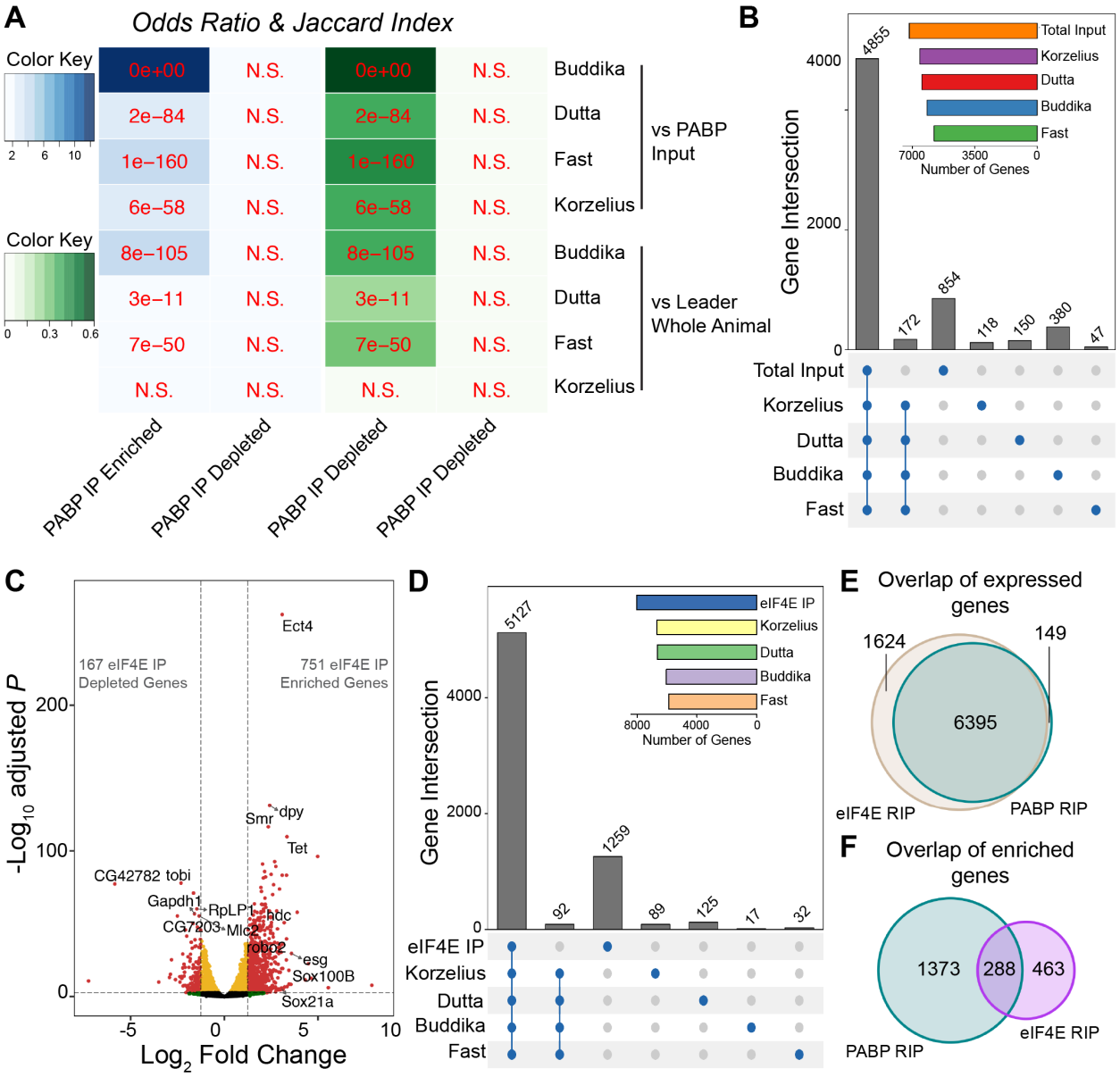

Figure S6: I-KCKT based RIPs identifies genes expressed in intestinal progenitors. (A) Heatmaps of odds ratio (in blue) and Jaccard index (in green) values for pairwise comparisons of PABP IP enriched or PABP IP depleted genes against input normalized FACS-based progenitor RNA-seq. Two sources of input data have been used for FACS data normalization: Total input of the PABP experiment, or female whole animal dataset from Leader *et al.,* 2017. Numbers on each colored box show the p-value for each overlap based on Fisher's exact test. N.S.: Not significant. (B) Upset plot showing the overlap of moderately expressed genes identified by FACS based methods

798 and total PABP IP input. Only a select set of meaningful overlaps are shown for
799 simplicity. The number above each bar shows the precise size of each intersection.
800 Note that 854 genes were uniquely present in the input, but not in any of the FACS
801 based datasets. (C) Volcano plot of differentially expressed genes from comparison of
802 eIF4E IP to total input from the PABP experiment. Each dot represents a single gene.
803 Yellow indicates a false discovery rate adjusted p-value (FDR) < 0.05 and a Log_2 fold
804 change > 1 or < -1. Green indicates Log_2 fold change > 1 or < -1 and an FDR >= 0.05.
805 Red indicates an FDR < 0.05 and log_2 fold change > 1 or < -1. A selected set of
806 significantly changed genes have been labeled. (D) Upset plot showing the overlap of
807 moderately expressed genes identified by eIF4E RIP-seq or FACS based methods.
808 Only a selected set of overlaps are shown for simplicity. Number above each bar shows
809 the precise size of each intersection. (E-F) Venn diagram of (E) moderately expressed
810 genes identified by eIF4E or PABP RIP-seq methods or (F) PABP or eIF4E IP enriched
811 genes compared to total input (FDR < 0.05 and log_2 fold change > 1). Only moderately
812 expressed genes were considered for the analyses shown in B, D and E. A gene is
813 defined as moderately expressed, if the TMM normalized expression value is greater
814 than 10 in all replicates. eIF4E IP indicates data from I-KCKT-based eIF4E RIP-seq.
815 Buddika, Dutta, Fast and Korzelius indicate data from RNA-seq of FACS isolated
816 progenitors from [2, 23, 24, 30], respectively.
817

818 **Supplementary Tables**

819 **Table S1: Fly strains used in this study**

Figure	Panels	Genotypes of flies used in each panel
Fig. 1	B, H	{tub-KDRT>-dSTOP-KDRT>-Gal4::p65^{1156}}attP40 / + ; {20XUAS-6XGFP}attP2 ; {βTry-KD::PEST^{1105}}attP2
	C, I	{tub-KDRT>-dSTOP-KDRT>-Gal4::p65^{1156}}attP40 / + ; {20XUAS-6XGFP}attP2 ; {θTry-KD::PEST^{1106}}attP2 / +
	D, J	{tub-KDRT>-dSTOP-KDRT>-Gal4::p65^{1156}}attP40 / + ; {20XUAS-6XGFP}attP2 ; {κTry-KD::PEST^{1110}}attP2 / +
	E, K	{tub-KDRT>-dSTOP-KDRT>-Gal4::p65^{1156}}attP40 / + ; {20XUAS-6XGFP}attP2 ; {CG18404-2.6kb-KD::PEST^{1108}}attP2 / +
	F, L	{tub-KDRT>-dSTOP-KDRT>-Gal4::p65^{1156}}attP40 / + ; {20XUAS-6XGFP}attP2 ; {CG18404-0.5kb-KD::PEST^{1109}}attP2 / +
	G, M	{tub-KDRT>-dSTOP-KDRT>-Gal4::p65^{1156}}attP40 / + ; {20XUAS-6XGFP}attP2 ; {CG10116-KD::PEST^{1107}}attP2 / +
Fig 2	A-E,P	{3Xgbe-smGFP::V5::nls}ZH2A, M{mira-His2A.mCherry.HA}Su(hw)attP18 / + ; {mira-KDRT>-dSTOP-KDRT>-Gal4::p65^{1126}}attP40 / P{UAS-Stinger}2 ; {CG10116-KD::PEST^{1107}}attP2 / +
	F-J,Q	{3Xgbe-smGFP::V5::nls}ZH2A, M{mira-His2A.mCherry.HA}Su(hw)attP18 / + ; {mira-KDRT>-dSTOP-KDRT>-Gal4^{1438}}attP40, P{tubP-Gal80[ts]}20 / P{UAS-Stinger}2 ; {CG10116-KD::PEST^{1107}}attP2 / +
	K-O, R,S	{3Xgbe-smGFP::V5::nls}ZH2A, M{mira-His2A.mCherry.HA} Su(hw)attP18 / {3Xgbe-Gal80}ZH-2A ; {mira-KDRT>-dSTOP-KDRT>-Gal4^{1438}}attP40, P{tubP-Gal80[ts]}20 / + ; P{UAS-Stinger}2; {CG10116-KD::PEST^{1107}}attP2 / +
Fig. 3	A, H	{mira-KDRT>-dSTOP-KDRT>-Gal4::p65^{1126}}attP40 / + ; {20XUAS-DSCP 6XGFP}attP2 / {CG10116-KD::PEST^{1107}}attP2
	B, H, I, J	{mira -KDRT>-dSTOP-KDRT>-Gal4^{1438}}attP40, P{tubP-Gal80[ts]}20 / + ; {20XUAS-DSCP-6XGFP} attP2 / {CG10116-KD::PEST^{1107}}attP2
	C, H	{Dl^{R24H06}-Gal80}ZH-2A / + ; {mira -KDRT>-dSTOP-KDRT>-Gal4^{1438}}attP40, P{tubP-Gal80[ts]}20 / + ; {20XUAS-DSCP-6XGFP} attP2 / {CG10116-KD::PEST^{1107}}attP2
	D, H	{3xgbe-Gal80}ZH-2A / + ; {mira -KDRT>-dSTOP-KDRT>-Gal4^{1438}}attP40, P{tubP-Gal80[ts]}20 / + ; {20XUAS-DSCP-6XGFP} attP2 / {CG10116-KD::PEST^{1107}}attP2
	E, H	P{GawB}NP5130 / + ; {20XUAS-DSCP 6XGFP}attP2 / +
	F, H	P{GawB}Dl$^{05151-G}$/ {20XUAS-DSCP 6XGFP}attP2
	G, H	P{Su(H)GBE-Gal4} / + ; {20XUAS-DSCP 6XGFP}attP2 / +
Fig. 4	A-N	{mira-KDRT>-dSTOP-KDRT>-Gal4^{1438}}attP40, P{tubP-Gal80[ts]}20 / + ; {CG10116-KD::PEST^{1107}}attP2 / P{UAS-dPF}D
Fig S1	A-F	{mira -KDRT>-dSTOP-KDRT>-Gal4^{1438}}attP40, P{tubP-Gal80[ts]}20 / P{lacW}esg^{k00606} ; {20XUAS-DSCP-6XGFP} attP2 / {CG10116-KD::PEST^{1107}}attP2
Fig S2	Top	P{GawB}NP5130 / P{UAS-Stinger}2 ;
	Bottom	{mira-KDRT>-dSTOP-KDRT>-Gal4::p65^{1126}}attP40 / P{UAS-Stinger}2 ; {CG10116-KD::PEST^{1107}}attP2 / +
Fig S3	A-F	{3Xgbe-smGFP::V5::nls}ZH2A, M{mira-His2A.mCherry.HA} Su(hw)attP18 /
Fig S4	A-O	{Dl^{R24H06}-Gal80}ZH-2A / + ; {mira -KDRT>-dSTOP-KDRT>-Gal4^{1438}}attP40, P{tubP-Gal80[ts]}20 / P{UAS-Stinger}2 ; + / {CG10116-KD::PEST^{1107}}attP2
Fig. S5	A,F,K,L	{mira-KDRT>-dSTOP-KDRT>-Gal4^{1438}}attP40, P{tubP-Gal80[ts]}20 / {UAS-FLAG::TEV::GFP^{1237}}attp40 ; {CG10116-KD::PEST^{1107}}attP2 / +

Fig. S5	B,G,K,L	{mira-KDRT>-dSTOP-KDRT>-Gal4^{1438}}attP40, P{tubP-Gal80[ts]}20 / + ; {CG10116-KD::PEST^{1107}}attP2 / {UAS-eIF4E::3xHA}ZH-86Fb (F000955*)*
	C,H,K,L	{mira-KDRT>-dSTOP-KDRT>-Gal4^{1438}}attP40, P{tubP-Gal80[ts]}20 / + ; {CG10116-KD::PEST^{1107}}attP2 / P{UAS-dPF}D
	D,I,K,L	{mira-KDRT>-dSTOP-KDRT>-Gal4^{1438}}attP40, P{tubP-Gal80[ts]}20 / {20XUAS-Lin-28::FLAG-HA}attP40 ; {CG10116-KD::PEST^{1107}}attP2 / +
	E,J,K,L	{mira-KDRT>-dSTOP-KDRT>-Gal4^{1438}}attP40, P{tubP-Gal80[ts]}20 / {20X UAS-FMRP::GFP::TEV::FLAG}attP40 ; {CG10116-KD::PEST^{1107}}attP2 /
Fig S6	A,E,F	{mira-KDRT>-dSTOP-KDRT>-Gal4^{1438}}attP40, P{tubP-Gal80[ts]}20 / + ; {CG10116-KD::PEST^{1107}}attP2 / {UAS-eIF4E::3xHA}ZH-86Fb (F000955*)*
	C, D, E,F	{mira-KDRT>-dSTOP-KDRT>-Gal4^{1438}}attP40, P{tubP-Gal80[ts]}20 / + ; {CG10116-KD::PEST^{1107}}attP2 / P{UAS-dPF}D

820

821

822 **Table S2: Oligos used in this study**

823 Note: Oligos used in Gibson Assembly are 50-60 nucleotides (nts) in length with the 5'

824 nts encoding plasmid sequence and the 3' nts (**in Bold**) encoding amplicon sequence.

No.	Sequence	Additional Information
3431	ATGCGCACCCGTGGCCAGGGCCGCAAGCTT**CGTCTAAGTGTGACTGATCCTGAAAGGGTT**	With 3432, amplifies 3.4kb *delta* enhancer
3432	GCCTCTATTTATACTCCGGCGCTCGACGTC**CGGAGACATCTGCTGGTGGAGGACATTATG**	With 3431, amplifies 3.4kb *delta* enhancer
3433	CATTATCAGACAAATGTCTGATATCGTTTCTCGAG**AATCAAAATGAAGCTGCTGAGTAGT**	With 3434, amplifies Gal4::p65
3434	AAGTAAGGTTCCTTCACAAAGATCCTCTAGA**TTAGGAGCTTATCTGGCTCAGCAAAGCGG**	With 3433, amplifies Gal4::p65
3437	ATGCGCACCCGTGGCCAGGGCCGCA**TGCCAGCACAGGCGGAACCCACAGCCAGGC**	With 3438, amplifies 3.4kb *βTry* enhancer
3438	CTATTTATACTCCGGCGCTCGACGT**GCGGTACTTCTTTCCGTTTTGGCCTGCGCC**	With 3437, amplifies 3.4kb *βTry* enhancer
3439	ATGCGCACCCGTGGCCAGGGCCGCA**CTAACAGCATCTAAGCTGGTACCCAGTAGG**	With 3440, amplifies 1.6kb *θTry* enhancer
3440	CTATTTATACTCCGGCGCTCGACGT**GCAGACATTTATAACTTTCCATCAGGCGCG**	With 3439, amplifies 1.6kb *θTry* enhancer
3441	ATGCGCACCCGTGGCCAGGGCCGCA**CCGCCCCAATTCGTCCGAATACCTAAGCTG**	With 3442, amplifies 1kb *CG10116* enhancer
3442	CTATTTATACTCCGGCGCTCGACGT**TATTCGTCTGAGGCATTCCTTAAGAGCTCG**	With 3441, amplifies 1kb *CG10116* enhancer
3443	ATGCGCACCCGTGGCCAGGGCCGCA**GGCAGGCGATTGTTGCCCAATGGAATGCCC**	With 3444, amplifies 2.6kb *CG18404* enhancer
3444	CTATTTATACTCCGGCGCTCGACGT**GCAATTCTTATCGTTTGGCTTATGTGGGAG**	With 3443, amplifies 2.6kb *CG18404* enhancer
3445	ATGCGCACCCGTGGCCAGGGCCGCA**CGTAGCTGGAGATGTAGCTAATGCTGCTGG**	With 3444, amplifies 0.5kb *CG18404* enhancer
3446	ATGCGCACCCGTGGCCAGGGCCGCA**TGGCGTACCTGAGGCCTTGGATCGATGCCG**	With 3447, amplifies 0.6kb *κTry* enhancer
3447	CTATTTATACTCCGGCGCTCGACGT**GGATTTCAGTTTAGACTTAGCTAGGTTGCG**	With 3446, amplifies 0.6kb *κTry* enhancer
3489	ATGCGCACCCGTGGCCAGGGCCGCA**GGTGAGTACCACGCTCTGCCATCAC**	With 3490, amplifies 2.6kb *mira* enhancer
3490	AGACAAATGTCTGATATCGTTTA**TTTCGAATTTGTTTTTTGGACTTTCGG**	With 3489, amplifies 2.6kb *mira* enhancer
3491	TTGCTGAGCCAGATAAGCTCCTAAT**GCTATTCCTTTGTAACAACTACTCT**	With 3492, amplifies 2.6kb *mira* enhancer
3492	ATCACGAGGCCCTTTCGTCTTCAAG**TGAATCTTAACGTCTGCGCAATTGC**	With 3491, amplifies 2.6kb *mira* enhancer
3626	ATGCGCACCCGTGGCCAGGGCCGCAAGCTT**AATTCGATATCAAGCTTGCACAGGTCCTGT**	With 3627, amplifies 2.6kb *tubulin* enhancer
3627	GCCTCTATTTATACTCCGGCGCTCGACGTC**GCGGATCTGATACCCCGGGCGGGTACCTTC**	With 3626, amplifies 2.6kb *tubulin* enhancer
4401	TGTCTGATATCGTTTCTCGAGAAGCTTAAC**GATCCGGGATCCCGTAAGCAAATAAACAAG**	With 4402, amplifies Gal4
4402	CGATAGAGTAGTTGTTACAAAGGAATAGCA**CCTACTCCTTCTTTGGGTTCGGTGGAGTAT**	With 4401, amplifies Gal4

825